

# Dynamic topography of the East European craton: Shedding light upon lithospheric structure, composition and mantle dynamics

Irina M. Artemieva

*Geological Institute, University of Copenhagen, Denmark*

Accepted 7 February 2007

Available online 11 April 2007

## Abstract

Most of the East European Craton lacks surface relief; however, the amplitude of topography at the top of the basement exceeds 20 km, the amplitude of topography undulations at the crustal base reaches almost 30 km with an amazing amplitude of *ca.* 50 km in variation in the thickness of the crystalline crust, and the amplitude of topography variations at the lithosphere–asthenosphere boundary exceeds 200 km. This paper examines the relative contributions of the crust, the subcrustal lithosphere, and the dynamic support of the sublithospheric mantle to maintain surface topography, using regional seismic data on the structure of the crystalline crust and the sedimentary cover, and thermal and large-scale P- and S-wave seismic tomography data on the structure of the lithospheric mantle. For the Precambrian lithosphere, an analysis of  $V_p/V_s$  ratio at 100, 150, 200, and 250 km depths does not show any age-dependence, suggesting that while  $V_p/V_s$  ratio can be effectively used to outline the cratonic margins, it is not sensitive to compositional variations within the cratonic lithosphere.

Statistical analysis of age-dependence of velocity, density, and thermal structure of the continental crust and subcrustal lithosphere in the study area (0–62E, 45–72N) allows to link lithospheric structure with the tectonic evolution of the region since the Archean. Crustal thickness decreases systematically with age from 42–44 km in regions older than 1.6 Ga to 37–40 km in the Paleozoic–Mesoproterozoic structures, and to *ca.* 31 km in the Meso-Cenozoic regions. However, the isostatic contribution of the crust to the surface topography of the East European Craton is almost independent of age (*ca.* 4.5 km) due to an interplay of age-dependent crustal and sedimentary thicknesses and lithospheric temperatures.

On the contrary, the contribution of the subcrustal lithosphere to the surface topography strongly depends on the age, being slightly positive (+0.3+0.7 km) for the regions older than 1.6 Ga and negative (–0.5–1 km) for younger structures. This leads to age-dependent variations in the residual topography, *i.e.* the topography which cannot be explained by the assumed thermal and density structure of the lithosphere, and which can (at least partly) originate from the dynamic component caused by the mantle flow. Positive dynamic topography at the cratonic margins, which exceeds 2 km in the Norwegian Caledonides and in the Urals, clearly links their on-going uplift with deep mantle processes. Negative residual topography beneath the Archean–Paleoproterozoic cratons (–1–2 km) indicates either a smaller density deficit (*ca.* 0.9%) in their subcrustal lithosphere than predicted by global petrologic data on mantle-derived xenoliths or the presence of a strong convective downwelling in the mantle. Such mantle downflows can effectively divert heat from the lithospheric base, leading to a long-term survival of the Archean–Paleoproterozoic lithosphere.

© 2007 Elsevier B.V. All rights reserved.

**Keywords:** continental lithosphere; continental crust; stability of cratons; depletion; subsidence; mantle flow; isostasy; secular evolution;  $V_p/V_s$  ratio

*E-mail address:* [Irina@geol.ku.dk](mailto:Irina@geol.ku.dk).

## 1. Introduction

The surface topography of the East European Craton (EEC) is far from being exciting. Surface erosion during a long-lasting (at least, since the Precambrian, Fig. 1b) development of most of the EEC as a stable platform has

delevelled the relief created by ancient processes of lithosphere deformation. Except for the Norwegian Caledonides, where some peaks rise to 2 km, most of the present-day EEC is flat with topography undulation within the 0–200 m range (Fig. 1a). However, the lack of relief does not mean the lack of a complicated

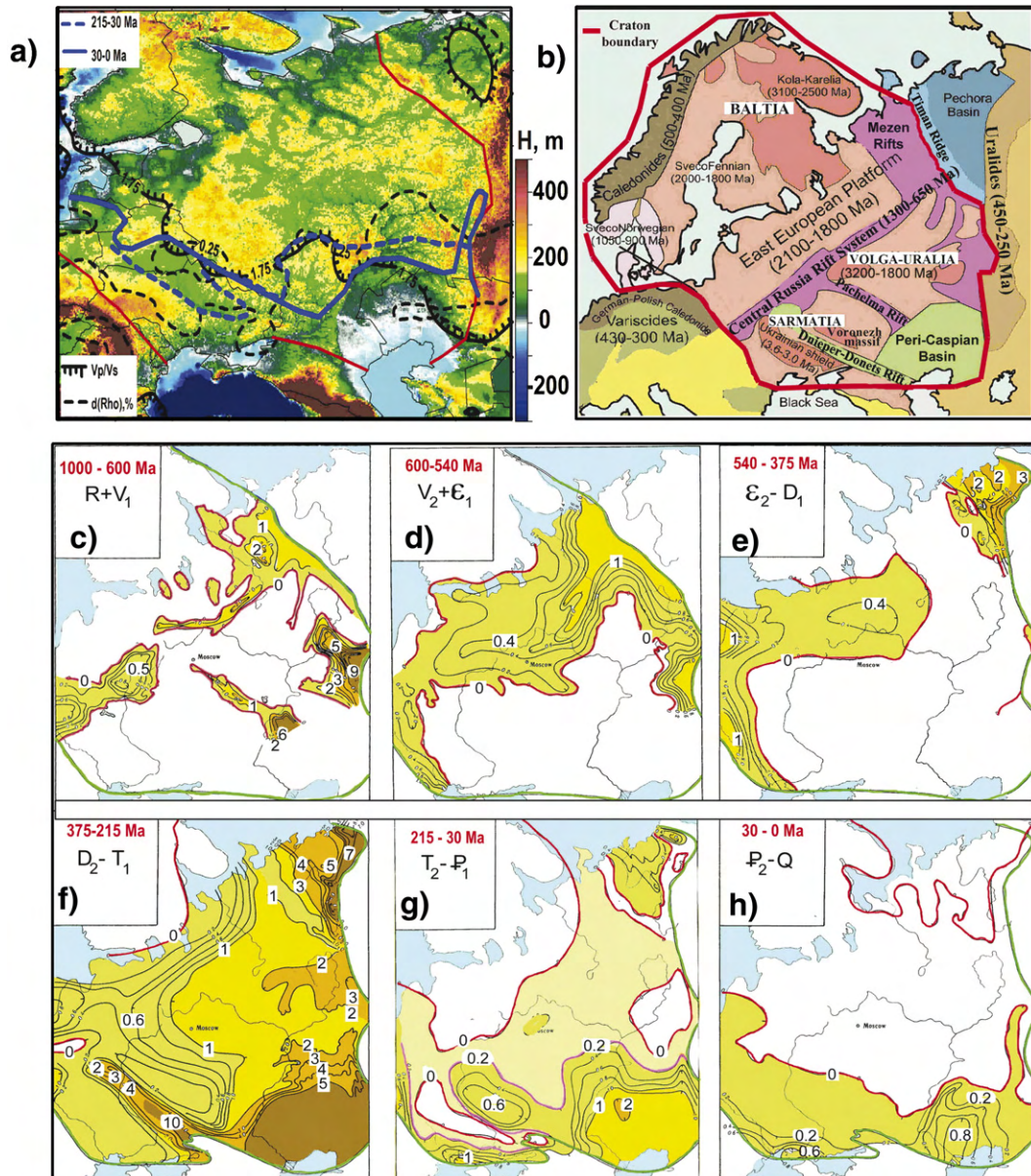


Fig. 1. Topography (a) based on a 2' compilation of global digital topography and bathymetry data ETOPO2 (NOAA, 2001), tectonic setting (b, after Artemieva et al., 2006), and subsidence history (c–h, after Nalivkin, 1976) of the East European Craton. Red line in (a, b) shows the craton boundaries. Blue lines in (a) — NE boundary of the areas subsiding during the Meso-Cenozoic (dashed line, based on (g)) and of the area of Neogene, on-going subsidence (solid line, based on (h)). Black lines in (a) — NE boundaries of compositional transition in the subcrustal lithosphere (solid hatched — based on Vp/Vs ratio at 150 km depth, see caption to Fig. 5; dashed — derived from temperature-corrected lithospheric buoyancy, after Artemieva, 2003; Artemieva et al., 2006). Note that regions of Meso-Cenozoic subsidence correlate well with the compositional boundary in the cratonic lithosphere.

tectonic history, which is vividly reflected in the topographies of the basement top, major crustal interfaces, crustal base, and the lithosphere–asthenosphere boundary. The geometry of these boundaries depends critically on the structure, composition, and thermal regime of the crust and the subcrustal lithosphere.

The goal of the present study is to unravel the complicated links between the topography of the intra-lithospheric interfaces and the tectonic evolution of the EEC over more than 3.5 Ga and to evaluate the contributions of different lithospheric layers to the surface topography signal. Compared to an earlier study (Artemieva, 2003), where the contribution of the lithospheric mantle to surface topography was calculated by subtracting crustal buoyancy from the observed surface topography, and thus included the isostatic contribution of both the lithospheric and the sublithospheric mantle, the present study separates the dynamic support of the sublithospheric mantle (dynamic topography) from the lithospheric buoyancy. This allows to examine the links between the present-day tectonic processes in Europe (partly related to the on-going tectonic deformation of the European lithosphere associated with the collision of the Eurasian, African, Scythian and the Arabian plates (Cloetingh et al., 2005)) and processes in the deep mantle.

## 2. Tectonic setting and subsidence history

The East European Craton includes a mosaic of tectonic structures, which forms the vast East European (Russian) Platform (EEP) and the Baltic Shield (Fig. 1b). The latter is subdivided into four major domains with different tectonic ages: the largely Archean Kola-Karelian province in the east, the Paleoproterozoic Sveco-Fennian province in the center, the Mesoproterozoic Sveco-Norwegian province in the south-west, and the Paleozoic Norwegian Caledonides along the western margin of the Baltic Shield.

The EEP is bordered at the west and east by two Paleozoic subduction zones (associated with the Trans-European suture zone (TESZ) (Nolet and Zielhuis, 1994) and the Uralides orogen (Hamilton, 1970), correspondingly) and by still active orogeny at the southern margin (the Caucasus) associated with the collision of the Arabian (Turkish) plate and the Scythian plate. Seismic tomography images of the Uralian (Poupinet et al., 1997) and the TESZ (Zielhuis and Nolet, 1994) subduction zones remain controversial, and while recent tomography studies of the Tethyan subduction image a slab underneath the Zagros suture zone (Hafkenscheid et al., 2006), no subduction zone has been imaged so far underneath the Caucasus.

Gorbatschev and Bogdanova (1993) proposed that the trans-cratonic Central Russia rift system (CRRS) and the Pachelma trough (rift) mark the suture zones along which three Archean-Paleoproterozoic terranes of the EEC (Baltia in the north, Sarmatia in the west, and Volga-Uralia in the east) were amalgamated in the Proterozoic (Fig. 1b). The oldest crust in Europe (in some areas >3.6 Ga) is known within the Dniester-Bugsky block of the Ukrainian shield and in the Voronezh Massif, both within the Sarmatian block of the EEC. Archean gneisses and granito-gneisses have been drilled in numerous deep (>3 km) prospecting boreholes in Volga-Uralia; unfortunately, accurate dating of the basement rocks is lacking for most of the EEP. The sedimentation history of the EEP indicates that the CRRS was reactivated at ~ 1.3–0.5 Ga (Fig. 1c–e).

The Devonian marks a new stage in the tectonic history of the EEP (Fig. 1f). A rapid sedimentation along the eastern margin of the EEP with the accumulation of up to 3 km of sediments over a period of *ca.* 100–150 Ma can be explained by a dynamic response (flexural bending) of the platform lithosphere to a Devonian west-dipping subduction associated with the Uralian orogeny (Mitrovica et al., 1996). Other important tectonic events in the Devonian took place in the southern parts of the EEP (Fig. 1b): the Peri-Caspian Basin began subsidence with the deposition of almost 10 km of sediments during the first 100–150 Ma of subsidence; the huge Dnieper–Donets rift system (filled with 15–20 km of sediments, Fig. 2a) cut through Sarmatia separating the Ukrainian shield and the Voronezh massif. A large volume of Devonian basalts erupted in the Dnieper–Donets rift system is commonly attributed to the presence of a mantle plume (*e.g.* Wilson and Lyashkevitch, 1996). It probably affected the lithospheric mantle of a large region in the southern EEP (Artemieva, 2003) and caused the initial subsidence of the Peri-Caspian Basin (a presence of the oceanic crust in the basin is suspected in the region of a triple junction of the Riphean Pachelma rift and the Devonian Sarpa and Central paleorifts). However, flexural bending of the cratonic lithosphere associated with the closure of the Paleo-Tethys and the development of subduction zones along its southern margin cannot be ruled out as a mechanism for the post-Devonian subsidence of the southern EEP.

The latest 200 Ma of the EEP tectonic history are marked by continuous, on-going subsidence of the southern parts of the platform with the accumulation of more than 20 km of sediments in the Peri-Caspian Basin (Figs. 1g–h and 2a). The origin of this on-going subsidence remains speculative. Good spatial correlation

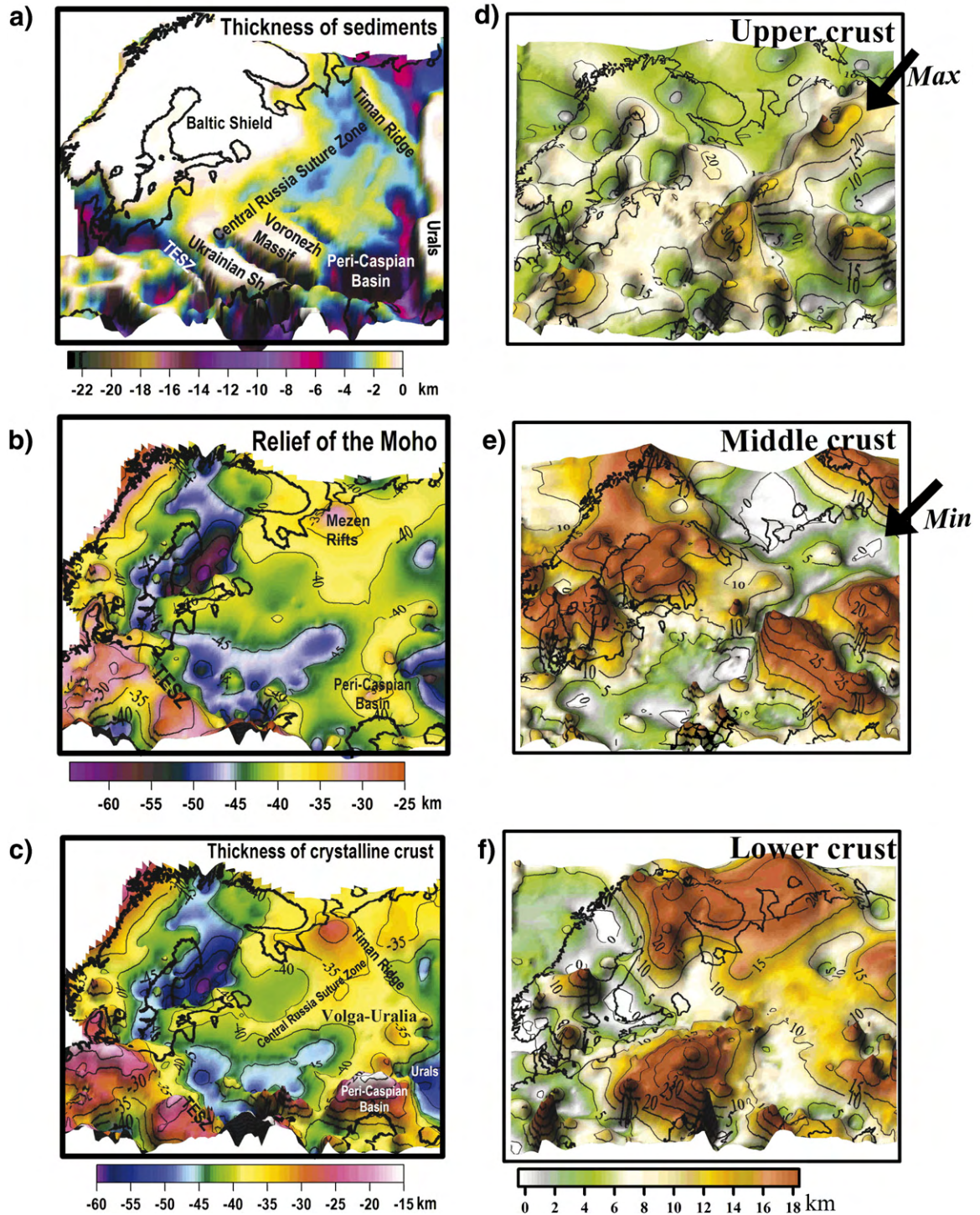


Fig. 2. Crustal structure of the East European Craton (see the text for references). (a) Basement relief; (b) Moho relief; (c) thickness of crystalline crust (difference between (b) and (a)); (d–f) thicknesses of three crustal layers, as defined by seismic velocities: upper crust  $V_p < 6.4$  km/s; middle crust  $V_p < 6.8$  km/s; lower crust  $V_p > 6.8$  km/s (calculated from crustal seismic profiles). Red arrows indicate the location of the Central Russia Rift System, which is well expressed in the thicknesses of the upper and middle crustal layers.

between the areas of Meso-Cenozoic subsidence, areas with a compositionally dense lithospheric mantle as constrained by lithospheric buoyancy and by Vp/Vs ratio in global and regional seismic tomography models (Fig. 1a) allowed to propose a compositional origin of the on-going platform subsidence due to metasomatic enrichment of cratonic lithosphere by Fe-rich heavy basaltic melts caused by the Devonian magmatism (Artemieva, 2003). However, this model does not account for a dynamic contribution of the mantle into the vertical movements of the southern EEP. This aspect is addressed in the present study.

### 3. Basement and Moho topography

#### 3.1. Thickness of sediments

The subsidence history of the EEC is reflected in the topography of the top of its basement (Fig. 2a), which has been mapped in numerous publications (including a map of the pre-Riphean basement of the EEP (Bronguleev, 1986), a map of the Hercynian basement of Ukraine (Sollogub et al., 1989), subsidence data for the Peri-Caspian basin (Nevolin and Kovylin, 1993), and compilations for other parts of the EEC (Kaban, 2001, 2002)). While the surface topography of the EEC is rather featureless, the topography of the top of the basement exceeds 20 km that is three times the height of the mt. Everest! The largest thickness of sediments is typical for the Paleozoic and Riphean rift zones within the EEC. The deepest basement depressions include the Peri-Caspian basin (*ca.* 22 km of sediments in the central part) and the Pripyat–Dnieper–Donets rift (20+ km of sediments in the south-central part (Donbas) and *ca.* 6–8 km in the northern part). The depressions of the Central Russia rift system and the Pachelma trough contain 3–5 km of sediments, while some depressions along the eastern margin of the EEP reach 5–8 km depth. Basement highs exist in numerous anticlines in Baltia (the Baltic shield), Sarmatia (the Ukrainian shield, the Voronezh Massif, the Belarus High), and Volga-Uralia (the Tokmovo and the Almetiev Domes). The thickness of sediments on these positive basement structures varies from near-zero values in the shield areas, to a few hundred meters in Sarmatia, and to 1.2–1.5 km in Volga-Uralia (Fig. 2a).

#### 3.2. Crustal thickness

Data on the crustal thickness of the EEC (Fig. 2) are based on the compilations of Pavlenkova (1988, 1996), Egorkin (1998), Kostyuchenko et al. (1999, 2004),

updated for seismic interpretations of the last decade for the TESZ (Sroda et al., 1999; Neprochnov et al., 2000; Bayer et al., 2002; Grad et al., 2002; Thybo et al., 2002; Wilde-Piorko et al., 2002; Janik et al., 2005; Grad et al., 2006), the north-western EEC (EUROBRIDGE SWG, 1999, 2000, 2001; Yliniemi et al., 2001; Kozlovskaya et al., 2002), the Ukrainian shield and the southern-western EEC (Grad and Tripolsky, 1995; Ilchenko and Bukharev, 2001; DOBREFraction'99 Working Group, 2003; Thybo et al., 2003; Stephenson, 2004), for Fennoscandia (Korsman et al., 1999; Bock et al., 2001; Korja et al., 2001; Alinaghi et al., 2003; Bruneton et al., 2004a,b; Sandoval et al., 2004; Korja and Heikkinen, 2005; Korja et al., 2006; Tiira et al., 2006), and for the Urals (Carbonell et al., 2000; Morozov, 2001).

The base of the crust displays strong topography undulations with an amplitude of up to 30 km (Fig. 2b). While the crustal thickness exceeds 60–65 km in south-western Finland (Tiira et al., 2006), it is only 30–32 km in the northern part of the Mezen rift province and 32–36 km in the central part of the Peri-Caspian basin, where the Devonian rifting has probably led to the formation of oceanic crust. Combined with the data on the thickness of sediments, thickness of the crystalline crust does not exceed 14–16 km in the central part of the Peri-Caspian basin (Fig. 2c), which makes the range of variations in the thickness of consolidated crust really amazing, *ca.* 50 km, among the largest documented for any craton of the world. The typical values of crustal thickness within most of the EEP are 42–45 km, and slightly less along the Proterozoic rifts of Central Russia (Kostyuchenko et al., 1999), but 47–48 km at the flanks of the Pachelma trough and 45–50 km in the Archean part of the Karelian province and in some blocks of the Ukrainian Shield. In the Sveconorwegian and Svecofennian provinces of Fennoscandia, crustal thickness typically varies from 32–36 to 42–45 km; however large thickness variations (36–65 km) are documented in the latter.

The statistical properties of the European crust reflect the dependence of the crustal structure on the tectonic history of the areas. The results are summarized in Table 1 for six time intervals (Archean, >2.5 Ga; late, middle, and early Proterozoic, >1.8 Ga, >1.0 Ga, >560 Ma, correspondingly; Paleozoic, >250 Ma, and Meso-Cenozoic) that correspond to the time of major tectonic events within the EEC.

Statistically, crustal thickness variations (*i.e.* depth to the Moho) in the Precambrian parts of the EEC, calculated from all available regional seismic studies, do not support an earlier conclusion on a thin Archean crust (Durrheim and Mooney, 1991): although the Archean crust of the EEC is slightly thinner than the

Table 1  
Statistical properties of the European crust and lithospheric mantle

Age	0–250 Ma *	250–580 Ma	580–900 Ma	0.9–1.6 Ga	1.6–2.5 Ga	>2.5 Ga	Average for the region*
Thickness of sediments, km	3.2±2.3	5.3±5.1	5.1±4.1	2.7±2.0	1.1±1.6	1.1±1.1	2.91±3.58
Crustal thickness, km	31.1±9.3	37.4±5.6	39.5±3.5	38.2±4.8	44.0±4.7	42.2±5.1	38.9±8.0
Average <i>in situ</i> basement density, g/cm <sup>3</sup>	2.894±0.089	2.887±0.052	2.897±0.037	2.902±0.041	2.913±0.035	2.910±0.035	2.90±0.05
Average <i>in situ</i> crustal density, g/cm <sup>3</sup>	2.835±0.056	2.844±0.055	2.853±0.034	2.872±0.040	2.901±0.040	2.897±0.038	2.87±0.05
Crustal density at SPT, g/cm <sup>3</sup>	2.866±0.051	2.878±0.055	2.884±0.033	2.900±0.042	2.930±0.040	2.922±0.038	2.90±0.05
Average <i>in situ</i> basement velocity, km/s	6.56±0.30	6.54±0.18	6.58±0.13	6.59±0.14	6.63±0.12	6.62±0.12	6.59±0.18
Moho temperature, °C	818±140	658±146	616±68	545±92	556±90	484±86	585±121
Temperature gradient in lith. mantle, °C/km	9.4±2.7	8.1±1.7	7.6±0.4	6.6±1.4	5.7±0.9	4.9±0.6	7.1±2.3
Lithosphere thermal thickness, km	96±35	126±40	140±13	158±38	181±36	212±33	154±51
SPT density of the lith. mantle, g/cm <sup>3</sup>	3.39	3.39	3.37	3.36	3.34	3.33	3.36±0.02
<i>In situ</i> density of the lith. mantle, g/cm <sup>3</sup>	3.27±0.02	3.27±0.01	3.26±0.01	3.25±0.01	3.23±0.01	3.23±0.01	3.25±0.02
Crustal buoyancy, km	3.65±1.63	4.52±0.61	4.71±0.55	4.33±0.68	4.57±0.53	4.43±0.47	4.39±0.88
Buoyancy of the lith. mantle, km (for SPT $\rho=3.39$ g/cm <sup>3</sup> )	-0.85±0.69	-0.99±0.57	-1.124±0.23	-1.51±0.59	-1.71±0.61	-2.28±0.65	-1.43±0.77
Residual topography, km (for SPT $\rho=3.39$ g/cm <sup>3</sup> )	0.75±2.15	-0.33±1.39	-0.12±0.70	0.64±0.95	0.54±0.95	1.38±0.91	0.46±1.41
Buoyancy of the lith. mantle, km (for age-dependent density)	-0.85±0.69	-0.99±0.57	-0.54±0.17	-0.45±0.29	0.31±0.15	0.69±0.19	-0.26±0.77
Residual topography, km (for age-dependent lith. density)	0.75±2.15	-0.33±1.39	-0.70±0.66	-0.41±0.87	-1.48±0.81	-1.59±0.64	-0.72±1.47
Vp/Vs (at 100 km depth)	1.71±0.04	1.74±0.05	1.70±0.02	1.71±0.04	1.69±0.04	1.69±0.03	1.71±0.04
Vp/Vs (at 150 km depth)	1.78±0.03	1.74±0.04	1.73±0.03	1.72±0.03	1.72±0.03	1.72±0.02	1.73±0.04
Vp/Vs (at 200 km depth)	1.82±0.03	1.79±0.03	1.79±0.01	1.77±0.03	1.78±0.03	1.77±0.02	1.79±0.03
Vp/Vs (at 250 km depth)	1.84±0.03	1.83±0.02	1.82±0.01	1.81±0.02	1.82±0.03	1.81±0.02	1.82±0.03

\* Note that data for the Meso-Cenozoic regions may not be representative of the entire western Europe (statistics restricted to the continental crust within 0–62E, 45–72N). SPT=standard pressure–temperature (i.e. at room conditions).

Paleoproterozoic crust (42.2 km and 44.0 km, correspondingly), statistically they are undistinguishable (Table 1). Instead, a strong trend in thinning of the crust with age is evident from the statistical analysis of available seismic data. Crustal thickness systematically decreases from 42–44 km in the oldest blocks of the EEC (>1.6 Ga) to 37–40 km in the Paleozoic–Mesoproterozoic structures, and to *ca.* 31 km in the Meso-Cenozoic regions. Similar trend is evident for the thickness of the crystalline crust, with the corresponding values of 41–43 km, 32–35 km, and *ca.* 28 km. Note that the statistics for the Meso-Cenozoic regions may not be representative of the entire West-European area, since the region of the study included only the continental crust within the quadrangle 0–62E, 45–72N. Furthermore, a large scatter for the Meso-Cenozoic crust is caused by a highly heterogeneous crustal structure of tectonically young regions, which include sedimentary basins, rift zones, and collisional orogens with the associated subduction zones.

Within the EEC, a striking correlation between the topography of the inter-crustal interfaces and the tectonic history is observed (Fig. 2, d–e). For example, the Central Russia rift system is clearly expressed in the thicknesses of the upper and middle crustal layers (Kostyuchenko et al., 1999; Artemieva, 2003): while the thickness of the former is *ca.* 15 km (probably due to magmatic additions during the Riphean rifting), the latter is thinned to less than 5 km. By contrast, the Archean blocks of the EEC are characterized by a thick (in many areas exceeding 20 km in thickness) high-density, high-velocity lower crust (Fig. 2f).

#### 4. Topography of the lithosphere–asthenosphere interface

##### 4.1. Thermal lithosphere

Similarly to the crustal structure, the lithosphere–asthenosphere boundary beneath the EEC exhibits a

strong relief (Figs. 3d and 5f). Good coverage of high-quality borehole heat flow measurements allows calculation of the lithospheric geotherms (Fig. 3) and estimation of thickness of the thermal lithosphere, defined here as the depth where the continental geotherms intersect the 1300 °C mantle adiabat. The details related to model assumptions and parameterization can be found elsewhere (e.g. Artemieva and Mooney, 2001). Sensitivity analysis shows that for the EEC the model uncertainties are *ca.*  $\pm 50$  °C for Moho temperatures,  $\pm 100$  °C for temperatures in the subcrustal lithosphere, and *ca.*  $\pm 25$  km for the lithospheric thickness (Artemieva, 2003; Artemieva et al., 2006).

The statistical analysis indicates a systematic, almost linear, increase in lithospheric thickness from Cenozoic to Archean structures (Fig. 4d), with a 200 km span in lithosphere thickness values. Reassessment of the thermal model (Artemieva, 2003) indicates that the

largest values (*ca.* 250–275 km) are estimated for the Kola-Karelian province and some parts of Volga-Uralia. Both Riphean and Devonian rifts are well expressed in the topography of the lithosphere–asthenosphere boundary, with the lithospheric thickness being in the range of 160–180 km and 120–140 km, respectively. The trend for the age-dependence of Moho temperatures is weak, especially for the Precambrian crust, due to large variations in the crustal thickness (Fig. 4a,c). Note that the transition from the craton to Phanerozoic Western Europe is marked by a sharp change in the deep thermal regime (Fig. 3).

#### 4.2. Seismic lithosphere

Large-scale seismic tomography models support the existence of large undulations of the lithosphere–asthenosphere boundary beneath the EEC (Fig. 5f).

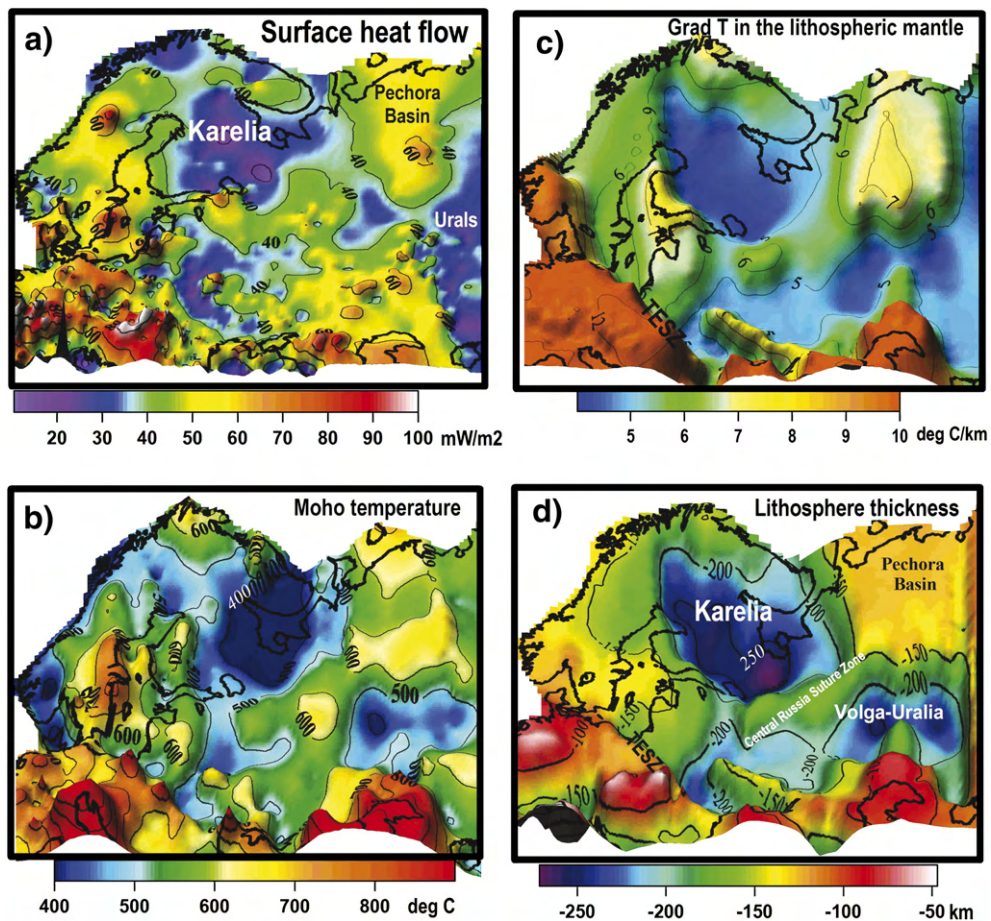


Fig. 3. Thermal regime of the East European Craton. (a) Surface heat flow (based on an updated global heat flow compilation, after Pollack et al., 1993); (b) temperatures at the base of the crust; (c) temperature gradient in the subcrustal lithosphere; (d) lithosphere thermal thickness (b–d are based on the TC1 global thermal model, Artemieva, 2006).

Although the lateral resolution of the global surface-wave tomography model (Shapiro and Ritzwoller, 2002) does not exceed 500–1000 km, it shows the same major features as the higher-resolution thermal model (Fig. 3d). Note, however, that seismic lithosphere is

systematically thicker (by *ca.* 50 km) than thermal lithosphere. This difference corresponds to the thickness of the transition zone between mantle layers with purely conductive and purely convective heat transfer (the former defines the thermal lithosphere). Furthermore, the

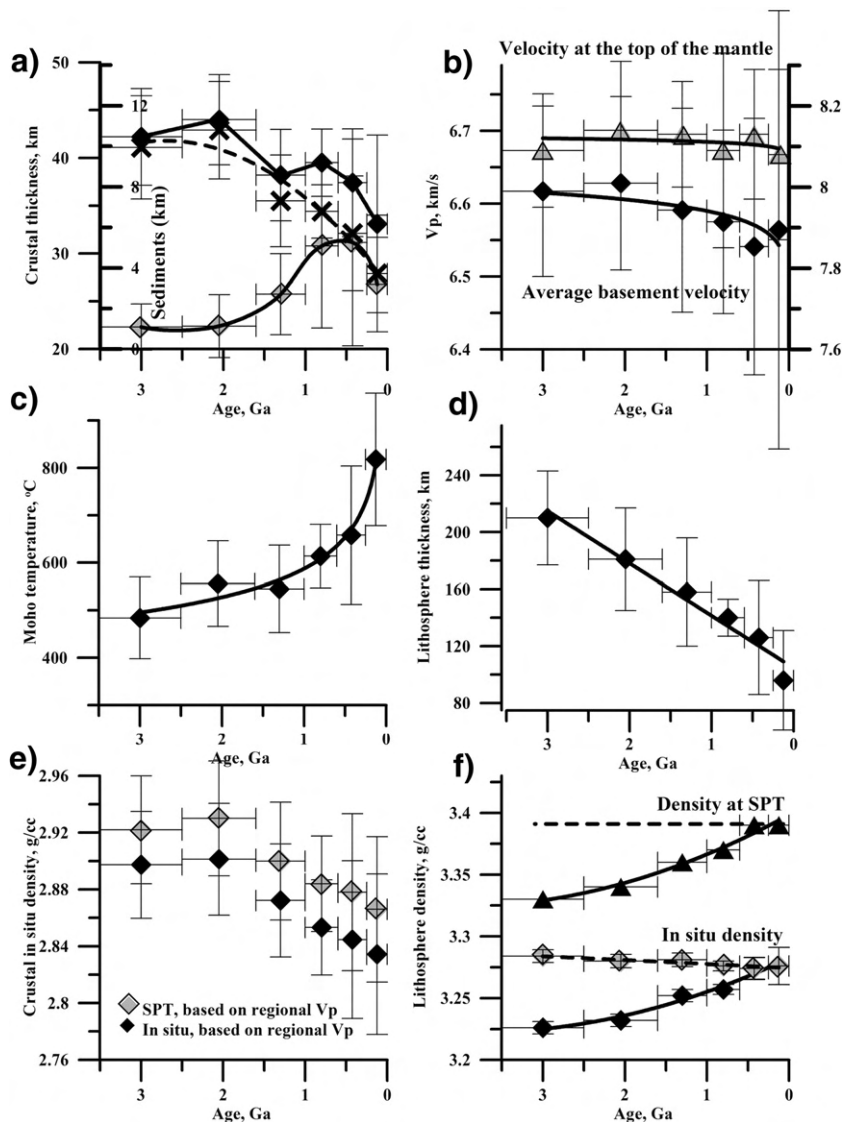


Fig. 4. Statistical properties of the European lithosphere (0–62E, 45–72N) for the Archean, late, middle, and early Proterozoic, Paleozoic, and Meso-Cenozoic. Horizontal axes in all plots — tectono-thermal age based on a  $1^\circ \times 1^\circ$  global model TC1 (Artemieva, 2006); horizontal bars indicate the time span used for averaging. Vertical bars show standard deviation of the parameters. Data sources for (a–d) are the same as for Figs. 2 and 3. (a) Crustal thickness (black diamonds), depth to the top of the basement (gray diamonds), and thickness of the crystalline crust (crosses and dashed line) calculated from published seismic interpretations for the region. (b) Average Vp velocity in the crystalline crust (black diamonds, left axis) and at the top of the mantle (gray triangles, right axis). (c) Temperatures at the base of the crust calculated from heat flow data and complemented by the TC1 model where borehole measurements are absent (Artemieva, 2006). (d) Lithosphere thermal thickness (Artemieva, 2003, 2006). (e) Average crustal density within the EEC (compare with Fig. 7c for the spatial patterns). Black diamonds — *in situ* densities converted from seismic velocities determined by regional seismic studies. Gray diamonds — the same, recalculated to room temperature. (f) Average density of the lithospheric mantle (compare with Fig. 7d–e for the spatial patterns). Upper curves — density at SPT (standard pressure–temperature, *i.e.* room) conditions; dashed line — for constant SPT density of 3390 kg/m<sup>3</sup>; solid line and triangles — typical SPT values measured on mantle xenoliths (*e.g.* Poudjom Djomani *et al.*, 2001). Lower curves and diamonds — *in situ* density calculated for the upper curves accounting for temperature variations in the lithosphere.

base of the seismic lithosphere (defined by a decrease in seismic velocities) has a diffuse character associated with high-temperature relaxation and partial melting (Anderson, 1989).

#### 4.3. Compositional lithosphere

A combined interpretation of P- and S-wave seismic tomography models allows to speculate on the properties of the upper mantle (Fig. 5, a–e). P-wave velocity perturbations are based on the tomography models of Piromallo and Morelli (2003) and of Bijwaard and Spakman (2000) recalculated to absolute velocity by scaling by the *ak135* model (Kennett and Engdahl, 1991). Both of these models have high lateral resolution ( $\sim 100$  km) in western Europe due to a good coverage of events and stations and low lateral resolution (500–1000 km) for most of the EEP (in particular, the NE part of the EEP has the lowest resolution leading to a large uncertainty of  $V_p/V_s$  ratios for this region). The vertical resolution of P-wave tomography models is low compared to surface-wave tomography, since body waves have an almost vertical propagation and sample the entire mantle. S-wave velocity perturbations are based on the global model of Shapiro and Ritzwoller (2002) for the Rayleigh-wave phase velocities, which has a vertical resolution of 50–100 km for the upper 250 km and a lateral resolution of *ca.* 500–1000 km. The S-wave velocity model is best resolved for the depth interval of 150–200 km, where the effect of the crust is weak but the vertical resolution is still significant.

Fig. 5, a–d can be interpreted in terms of compositional anomalies in the lithosphere of Europe, since the  $V_p/V_s$  ratio is thought to be more sensitive to compositional than to temperature variations (*e.g.* Lee, 2003). A statistical analysis of  $V_p/V_s$  variations within the European upper mantle (Fig. 5e) shows high variability of  $V_p/V_s$  at 100 km depth (in particular, for the Paleozoic and Mesoproterozoic regions), which is likely to be caused by the crustal effect, not entirely removed in the P- and S-wave tomography models. For the deeper mantle, almost no age-dependence of  $V_p/V_s$  ratio is observed for Precambrian regions older than 0.9 Ga. Since lithosphere younger than 0.9 Ga is, statistically, thinner than 150 km (Table 1), high  $V_p/V_s$  ratios for the lithosphere of this age are associated with the sublithospheric mantle. It implies that while  $V_p/V_s$  ratio can be efficiently used to outline the margins of cratonic lithosphere, it does not allow to distinguish lithospheric blocks of different ages (and composition) within the Precambrian cratons.

### 5. Quantifying crustal and mantle contributions to the surface topography

Huge variations in the thicknesses of the sedimentary cover ( $> 20$  km), of the crystalline crust (*ca.* 50 km), and of the lithosphere (*ca.* 200 km) combined with an almost complete absence of surface relief within the EEC make it intriguing to analyze the relative contributions of the crust, the subcrustal lithosphere, and the sublithospheric mantle to maintaining regional isostasy. Following Lachenbruch and Morgan (1990), the isostatic contributions of the crust and the subcrustal lithosphere to topography can be quantified, provided their structure (thickness and average *in situ* density) is known. The calculations are based on the following assumptions: (a) the isostatic balance is achieved at the base of the lithosphere; (b) surface topography results from the sum of the crustal and lithospheric buoyancies and a contribution of the dynamic topography (the latter effect was neglected in the previous study (Artemieva, 2003)); (c) the asthenosphere has a uniform density; (d) density variations within the lithosphere depend on its composition and temperature. Under these assumptions, the crustal contribution to the surface topography (crustal buoyancy  $B_c$ ) is caused by variations in crustal thickness  $H_c$  and crustal density:

$$B_c = \frac{\rho_a - \rho_c}{\rho_a} H_c, \quad (1)$$

where  $\rho_a$  is density of asthenosphere and  $\rho_c$  is the average *in situ* density of the crust (Fig. 6). Similarly, lithospheric contribution to the surface topography (*i.e.* lithospheric buoyancy  $B_l$ ) depends on the thickness of the subcrustal lithosphere  $H_l$  and the average density contrast between the asthenosphere and the lithosphere:

$$B_l = \frac{\rho_a - \rho_l}{\rho_l} H_l, \quad (2)$$

where  $\rho_l$  is mean density of the subcrustal lithosphere at *in situ* temperature and pressure:

$$\rho_l = \rho_o [1 - \alpha \Delta T + \beta \Delta P], \quad (3)$$

$\alpha = 3.5 \times 10^{-5} \text{ } ^\circ\text{C}^{-1}$  is the volume coefficient of thermal expansion,  $\beta$  is compressibility, and  $\rho_o$  is SPT density (at standard pressure–temperature, *i.e.* at  $T = 25 \text{ } ^\circ\text{C}$  and  $P = 1 \text{ atm}$ ) of the subcrustal lithosphere. For the lithospheric mantle, the pressure effect on densities as well as the temperature effect on thermal expansion are insignificant (*e.g.* Nisbet, 1984), in particular in comparison with uncertainties in densities, temperatures and thicknesses of the crust and the lithosphere (see Table 2

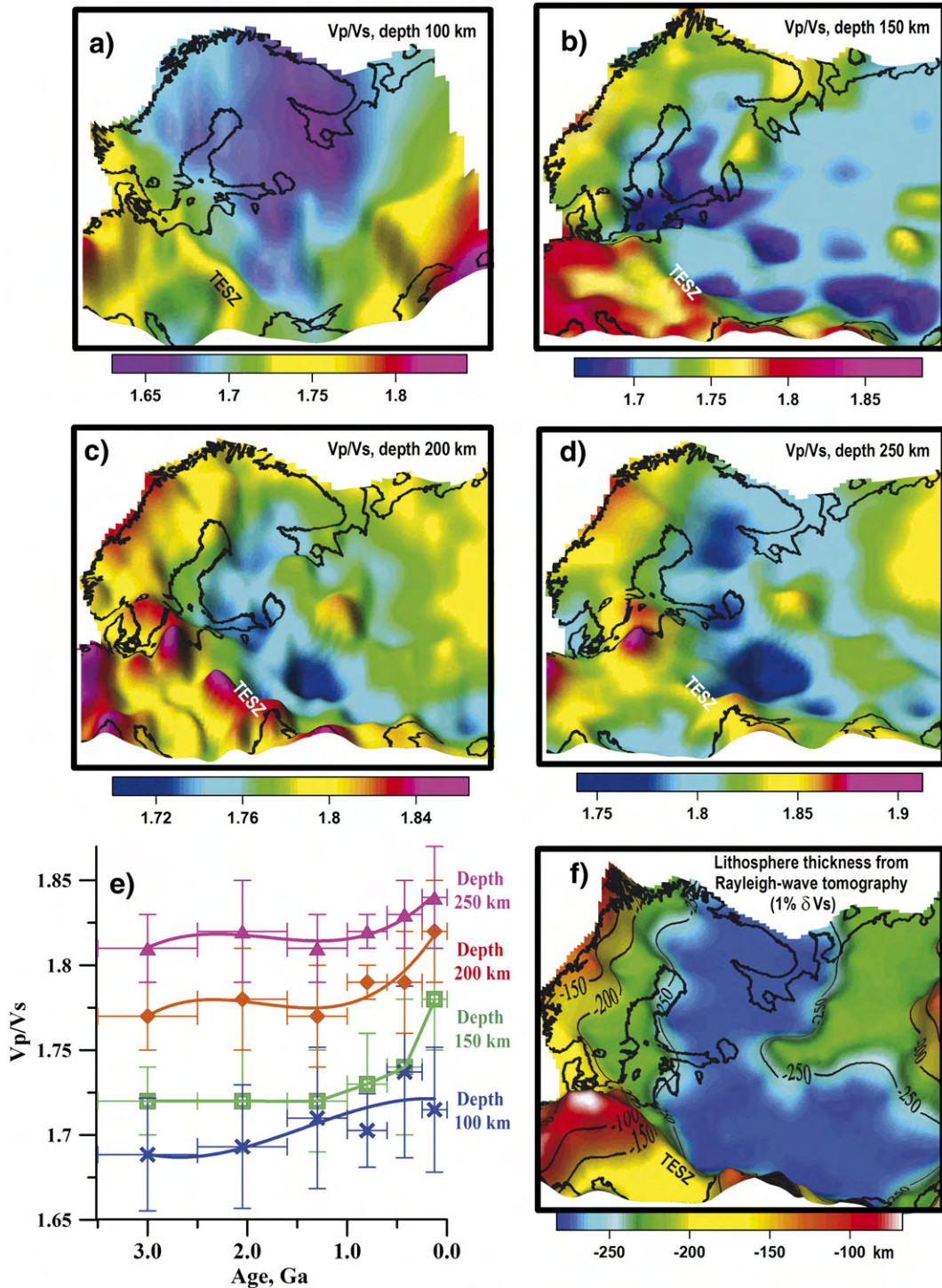


Fig. 5. (a–d) Vp/Vs ratio at 100, 150, 200, and 250 km depth (smoothed by Gaussian filtering), based on the tomography models of Bijwaard and Spakman (2000), Piromallo and Morelli (2003), Shapiro and Ritzwoller (2002). The maps reflect compositional anomalies in the lithosphere of Europe. See text for explanations. (e) Variation of Vp/Vs ratio as a function of tectono-thermal age of the lithosphere of Europe. (f) Depth to the lithosphere–asthenosphere boundary; here the base of the seismic lithosphere is defined by a 1% perturbation of Rayleigh-wave phase velocities (derived from the global model of Shapiro and Ritzwoller (2002) and interpolated with a low-pass filter) with respect to the global continental model *iaspei91* (Kennett and Engdahl, 1991).

and the section on the sensitivity analysis), and can be neglected.

The mean (*in situ*) lithospheric temperature can be considered as the arithmetic mean between the sub-crustal (Moho) temperature  $T_M$  and the asthenospheric temperature  $T_o$  (assumed here to be 1300 °C). Thus, a contribution of thermal expansion to density variations in the subcrustal lithosphere is specified by Moho temperatures (Figs. 3b and 4c):

$$\rho_1 = \rho_o \left[ 1 - \alpha \frac{T_M + T_o}{2} \right]. \quad (4)$$

The set of Eqs. (1)–(4) allows to calculate the contributions of the crust and the subcrustal lithosphere to the total topographic signal and to quantify the residual topography  $D$ , *i.e.* the topography which cannot be explained by the assumed structure of the crust and the subcrustal lithosphere, and which can, at least in part, originate from the dynamic contribution of the sublithospheric mantle (the dynamic topography) into the surface topography  $H_o$ :

$$D = H_o - B_c - B_l + \Delta. \quad (5)$$

Short-wavelength lateral variations of the residual topography can also reflect regionally compensated local lithospheric flexure related to the bending stresses or displacements on faults (Burov and Diament, 1995). In the cratonic regions, where the lithosphere is characterized by high values of flexural rigidity (and thus has large

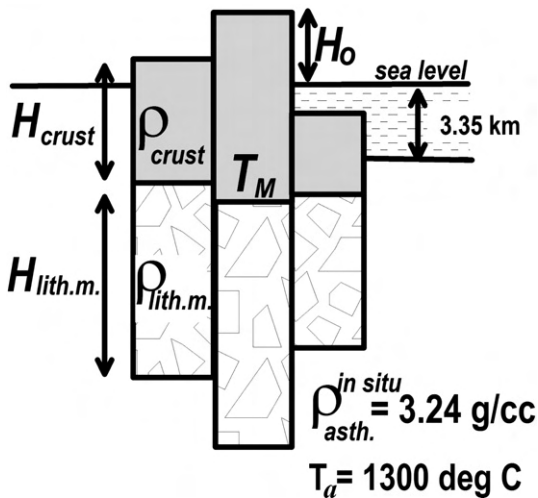


Fig. 6. Background for the buoyancy calculations (after Lachenbruch and Morgan, 1990). See text for explanations.

Table 2  
Sensitivity analysis

	Crustal buoyancy $B_c$ (km)	Lithospheric buoyancy $B_l$ (km)	Residual (dynamic) topography $D$ (km)
Moho temperature $T_M$ 100° higher	The same	0.20 km greater	0.20 km less
Crustal thickness $H_c$ 2 km greater	0.19 km greater	0.05 km greater	0.24 km less
Crustal density $\rho_c$ 0.05 g/cc less	0.55 km greater	The same	0.55 km less
Lithosphere thickness $H_c+H_l$ 20% less	The same	0.07 km greater	0.07 km less

values of elastic thickness, >60 km for most of the EEC (Pérez-Gussinyé and Watts, 2005)), this would correspond to a wavelength of few hundred kilometers. Note, however, that lateral resolution of the present study is effectively limited to 100–200 km by the areal coverage by seismic and borehole data, and thus for most of the EEC short-wavelength flexural contributions to the residual topography can be neglected.

The constant  $\Delta$  is the height of the sea level above the asthenosphere and it can be estimated for the oceanic lithosphere, where the bathymetry  $\varepsilon$  can be calculated from the Airy scheme of isostatic compensation:

$$\varepsilon = \frac{\rho_a - \rho_l}{\rho_a - \rho_w} L - \Delta. \quad (6)$$

Here  $L$  is lithospheric thickness,  $\rho_l$  — mean lithosphere density,  $\rho_w$  — water density. For an oceanic ridge all of these parameters can be estimated with greatest confidence (Lachenbruch and Morgan, 1990), and the constant  $\Delta \approx 3.35$  km for  $\rho_l = 2900 \text{ kg/m}^3$ ,  $\rho_a = 3240 \text{ kg/m}^3$ ,  $\rho_w = 1020 \text{ kg/m}^3$ ,  $L = 5.5$  km,  $\varepsilon = -2.5$  km.

Calculations of  $B_l$  (the isostatic contribution of lithospheric roots to the surface topography),  $B_c$  (the topography predicted from an isostatically balanced crust), and  $D$  (the dynamic topographic support of the sublithospheric mantle) require data on the surface topography, thickness and density of the crust, SPT density of the subcrustal lithosphere, lithospheric thickness, Moho temperatures, and density of the asthenosphere. A 2-minute global digital topography and bathymetry model of the Earth (Fig. 1a, NOAA, 2001) provides high-resolution data on the surface topography. Data on the crustal thickness and Moho temperatures were discussed earlier (Figs. 2b and 3b); for consistency, the depth to the lithosphere–asthenosphere boundary was based on thermal constraints (Fig. 3d) which,

besides, provide better lateral resolution than seismic tomography models. The choice of the other parameters is discussed in the following section.

## 6. Density structure of the crust and the upper mantle

### 6.1. Density of asthenosphere

The density of the asthenosphere is assumed to be constant beneath the different lithospheric blocks and, thus, an uncertainty in its true value may result only in a systematic shift of the results. For a pyrolite composition of the upper mantle, its SPT (*i.e.* at room conditions) density is in the range from 3370 to 3410 kg/m<sup>3</sup> (*e.g.*, Anderson, 1987; Irifune, 1987). In the present study a mean value of 3390 kg/m<sup>3</sup> is used, which is equivalent to an *in situ* asthenospheric density of 3240 kg/m<sup>3</sup> (for thermal expansion coefficient of  $3.5 \times 10^{-5} \text{ }^\circ\text{C}^{-1}$  and the potential temperature of the upper mantle of 1300 °C).

### 6.2. Density of the crust

The density structure of the entire continental crust is poorly known due to a large uncertainty in the genesis, composition and, as a result, density structure of its lower layer (Jordan, 1979; Rudnick and Fountain, 1995). A velocity–density conversion based on laboratory studies of crustal rocks provides estimates of crustal densities. In the present study, the average *in situ* density of the crystalline crust (Figs. 4e and 7a) was calculated from the average *in situ* basement Vp-velocities (see Section 3 for references), using the experimental relationship of Christensen and Mooney (1995) for the depth of 20 km, which approximately corresponds to the mean *in situ* pressure in the basement rocks. Note that Phanerozoic crust has significantly lower velocities (6.2–6.4 km/s) than the cratonic crust (6.6–6.8 km/s), and hence lower densities (Artemieva et al., 2006). The largest crustal velocities (>6.8 km/s) are observed in the Archean-Paleoproterozoic Kola-Karelia and the Ukrainian shields, which have the highest density of the crystalline crust (2950–3090 kg/m<sup>3</sup>) (Table 1). As a result, the *in situ* density contrast between the crystalline crust and the sublithospheric upper mantle differs remarkably between the cratonic and the Phanerozoic crust: *ca.* 500 kg/m<sup>3</sup> for the crust of western Europe, 300–350 kg/m<sup>3</sup> for most of the Precambrian crust, and as little as 150–250 kg/m<sup>3</sup> for some parts of the Baltic and the Ukrainian shields (Fig. 7a).

The sedimentary cover of the EEC ranges in thickness from near-zero values in the shield areas to more than 20 km in the southern parts of the platform affected by the Paleozoic tectono-magmatic activity (Fig. 2a). A vast amount of geophysical exploration studies combined with numerous borehole data from different parts of the EEP provides important information on regional (both lateral and vertical) variations in the density of sediments (see references in Yegorova et al., 1999; Kaban, 2001). The density of the sedimentary cover of the EEP ranges from 1900 to 2350 kg/m<sup>3</sup> in the Meso-Cenozoic sand and clay deposits (with the highest values in the Dnieper–Donets rift) through 2300–2550 kg/m<sup>3</sup> in the late Paleozoic clastics and carbonates in most of the EEP to 2800 kg/m<sup>3</sup> in the early Paleozoic effusives of the Dnieper–Donets rift and to 2850–2900 kg/m<sup>3</sup> in the Vendian–Cambrian carbonates of the Peri-Caspian basin. In regions, where the thickness of sediments exceeds 7–8 km, the compaction effect results in a density increase in the lowermost sediments to values close to crystalline rocks. Using a platform-wide compilation of data on lateral and vertical density variations in the sedimentary cover of the EEP (Podoba and Ozerskaya, 1975), the following relationship between the density of sediments  $\rho$  (in kg/m<sup>3</sup>) and their depth  $z$  (in km) was used in the present analysis to account for the pressure effect:

$$\rho = 2430 * z^{0.045}. \quad (7)$$

The depth  $z$  is assumed to be equal to 1/2 of the total thickness of sediments.

The map of the total crustal density (sediments plus crystalline crust) (Fig. 7b) differs considerably from the density (or velocity) map for the crystalline crust (Fig. 7a). In particular, a low total crustal density is characteristic for the major sedimentary basins of the EEC, including the Peri-Caspian basin, the Dnieper–Donets rift, the eastern Volga-Uralia, and the Central Russia rift system. In these regions the total crustal density contrasts with the asthenosphere by *ca.* 400–450 kg/m<sup>3</sup>. The smallest crust–mantle density contrast is observed in some parts of the Ukrainian shield, 250 kg/m<sup>3</sup> only.

Statistical analysis of the age-dependence of the total crustal density indicates that it systematically increases with age from *ca.* 2835 kg/m<sup>3</sup> in Meso-Cenozoic regions (2866 kg/m<sup>3</sup> at STP) to *ca.* 2900 kg/m<sup>3</sup> in the Archean-Paleoproterozoic crust (2920–2930 kg/m<sup>3</sup> at STP) (Table 1). For *in situ* values, a polynomial:

$$\rho_{in\ situ} = 2.824 + 0.05 * t - 0.008 * t^2 \quad (8)$$

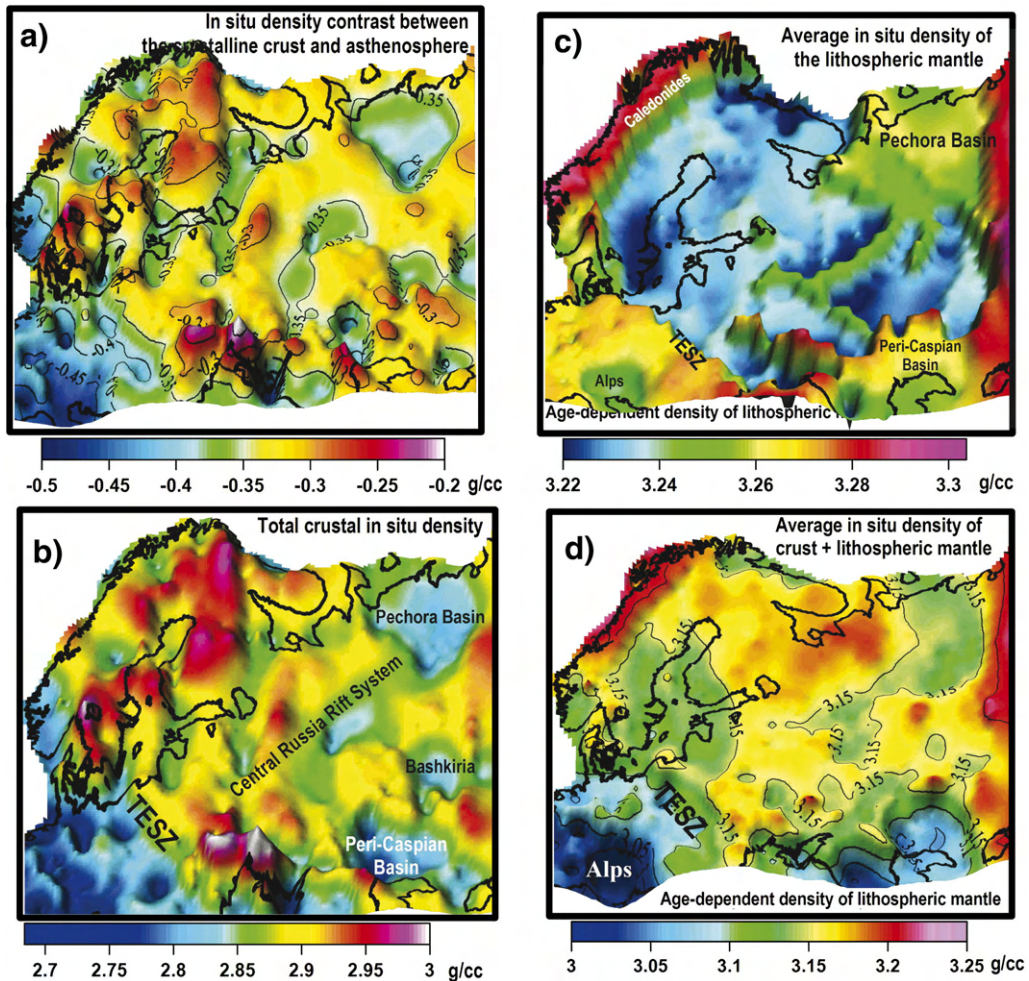


Fig. 7. Density structure of the European crust and lithospheric mantle. Data sources same as for Figs. 2 and 3. (a) Average *in situ* density contrast between the crystalline crust (calculated from average basement  $V_p$  velocity) and the asthenosphere. (b) Average *in situ* density of the entire crust (basement plus sediments). (c) *In situ* density of the lithospheric mantle calculated from the SPT density accounting for temperature variations in the lithosphere (Fig. 3b). The values are typical SPT values measured on mantle xenoliths from tectonic terranes of different ages (e.g. Poudjom Djomani et al., 2001). (d) Average *in situ* density of the entire lithospheric column (based on data in Figs. 3b, d, 7b, c). Note a sharp transition from Phanerozoic to the cratonic lithosphere.

provides the best fit, where  $\rho_{in situ}$  is the total *in situ* density of the crust (in  $t/m^3$ ) and  $t$  is tectono-thermal age of the crust in Ga (the latter value can be derived from the global continental model TC1, Artemieva, 2006). Density values at STP conditions (temperature effect removed) show a similar trend. The high total density of the early continental crust results from the absence of a sedimentary cover and from the large thickness of high-density lower crust (Fig. 2f), while the significant thickness of sediments and the absence of a high-velocity lower crust in the European Variscides result in a low total crustal density. Since the Central Russia rift system is well expressed in the structure of both the

crystalline crust (Fig. 2, d–e) and the sedimentary cover (Fig. 2a), it expresses itself as a distinct low-density crustal zone within the EEP (Fig. 7b).

### 6.3. Density of the subcrustal lithosphere

Numerous petrologic studies of craton and off-craton mantle-derived peridotite xenoliths indicate strong chemical heterogeneity of the lithospheric mantle beneath the continents with well-documented secular variations in its composition (e.g. Boyd, 1989; Pearson et al., 1995; Griffin et al., 1998, 1999). In particular, as compared to the convecting mantle, the ancient cratonic lithosphere is

depleted in basaltic components (quantified by  $mg\# = Mg / (Mg + Fe)$ ) due to the removal of Fe-rich melts. Off-craton peridotites have  $mg\#$  intermediate between the cratonic peridotites and the oceanic lithosphere (e.g. Pearson et al., 1995; Gaul et al., 2000), suggesting that not only the Archean but the Proterozoic lithosphere is depleted.

Since the density of the lithospheric mantle is essentially controlled by the olivine composition (e.g. Griffin et al., 1998), lithosphere depletion results in a density deficit, which is determined as the ratio of the density contrast between the lithospheric mantle and the asthenosphere to the density of the asthenosphere,  $\Delta\rho = (\rho_l - \rho_a) / \rho_a$ . In particular, an increase in  $mg\#$  with age results in a strong, almost linear, decrease in the density of the subcrustal lithosphere with age (e.g. Jordan, 1981), as indicated by density calculations based on the mean mineral compositions of the lithospheric mantle and experimental data on the densities of the end-member minerals (e.g. Boyd et al., 1993; Griffin et al., 1998; Gaul et al., 2000).

The results of earlier studies (Artemieva, 2003; Kaban et al., 2003) suggest that the density deficit in the lithospheric mantle may not necessarily correspond to the values expected from petrologic studies. To examine the competing roles of lithosphere depletion and the dynamic support of the mantle on surface topography, two end-member density models for the lithospheric mantle are used in the present study (Fig. 4f):

- (a) with the constant SPT density equal to the SPT density of asthenosphere (i.e.  $3390 \text{ kg/m}^3$ ) so that all *in situ* lateral density variations in the lithospheric mantle are solely of thermal origin;
- (b) with the age-dependent SPT density of the lithospheric mantle (Fig. 7c) with the values based on petrologic studies of peridotites from mantle xenoliths:  $3390 \text{ kg/m}^3$  for the Phanerozoic mantle,  $3360\text{--}3370 \text{ kg/m}^3$  for the Neo- and Mesoproterozoic mantle, and  $3300\text{--}3340 \text{ kg/m}^3$  for the Archean-Paleoproterozoic mantle (Table 1). These values correspond to 1.4–1.5%, 0.6–0.9% and 0% of depletion of the subcrustal lithosphere with respect to the underlying mantle. Thus in both density models, the Phanerozoic subcrustal lithosphere is assumed to have formed by conductive cooling of the convective mantle and have the same composition as the latter.

Following the results of Kaban et al. (2003), the compositional variations between the lithosphere of the same age are assumed to be small, and thus age-dependent density of the lithospheric mantle is the same for the lithosphere of the same age, while all density

variations in a lithospheric column are caused by thermal expansion. The tectono-thermal ages of the mantle are based on the global continental TC1 model constrained on a  $1^\circ \times 1^\circ$  grid (Artemieva, 2006), assuming that the ages of the lithospheric mantle and the overlying crust are essentially the same. Regional petrologic and seismic studies indicate that this assumption is generally valid at distances  $>100\text{--}200 \text{ km}$  from the terrane boundaries of different ages (e.g. BABEL Working Group, 1993; Clowes et al., 1998; Cook et al., 1999; Pearson, 1999).

Data on the Moho temperature (Fig. 3b) are used to correct SPT lithospheric density for thermal expansion and to calculate mean *in situ* density of the subcrustal lithosphere (Eq. (2), Figs. 4f and 7c). The resulting average *in situ* density of the entire lithospheric column (sediments, crystalline crust, and the lithospheric mantle assuming age-dependent SPT density) is shown in Fig. 7d. Although these values are not used in the further analysis, they provide important constraints for analysis of gravity data (that is outside the scope of this study). Intriguing features in Fig. 7d are the high total lithospheric densities in the Caledonides, the Uralides, and the Mezen Rift system and the low densities beneath the Baltic Sea, the Peri-Caspian Basin, and the Phanerozoic structures (western Europe and the Pechora Basin).

## 7. Crustal, lithospheric and dynamic contributions to the surface topography

### 7.1. Sensitivity analysis

In the present study, the isostatic contribution of the lithospheric mantle (lithospheric buoyancy) is calculated directly from data on the lithospheric thickness, temperature, and density (Eqs. (2)–(4)). Such an approach, as compared to an earlier study (Artemieva, 2003), allows to separate the dynamic support of the sublithospheric mantle (dynamic topography) from the isostatic contributions of the crust and the subcrustal lithosphere to the total topographic signal (Eq. (5)).

Five parameters control the results of the isostatic calculations (Eqs. (1)–(4)): data on the thicknesses and densities of the crust and lithospheric mantle, and temperature at the crustal base. The results of the sensitivity analysis are summarized in Table 2 for all of these parameters; variations in their values reflect the typical uncertainties in their estimates. The effect associated with the uncertainty of the density structure of the lithospheric mantle is not included, since the two density models used in the study (constant and age-dependent) illustrate the effect of possible density variations in the lithospheric mantle.

The uncertainty associated with the average crustal density has the strongest effect on the final results (up to 0.5 km), while results are much less sensitive to the uncertainties in crustal thickness and Moho temperatures (Table 2). The uncertainty in the lithospheric thickness alone has a weak effect on the solution, although in this case a change in Moho temperature will occur. On the whole, in the most unfortunate case when all uncertainties work in the same direction, the total uncertainty is *ca.* 0.75 km for the crustal buoyancy and *ca.* 0.25 km for the lithospheric buoyancy, leading to *ca.* 1 km for the residual (or dynamic) topography.

## 7.2. Crustal buoyancy

The isostatic contribution of the crust to surface topography (crustal buoyancy) depends on the crustal thickness and density (Eq. (1)). For a typical crustal *in situ* density of 2835–2900 kg/m<sup>3</sup> (Table 1) and crustal thickness of 40–42 km, the crustal contribution to the surface topography is *ca.* 4–5 km (Fig. 8a, c). Within the EEC, the crustal buoyancy varies from <3 km to *ca.* 5 km, locally reaching 6 km. Since the Phanerozoic crust is thin, but warm and light, while the cratonic crust is thick, but cold and dense, the interplay between lateral variations in the crustal thickness and crustal density results in a mosaic spatial pattern of the crustal buoyancy (Fig. 9a).

Fig. 8c–d show the statistical values of the crustal, lithospheric and dynamic (residual) contributions to the European topography as a function of tectono-thermal age, for a constant and age-dependent SPT densities of the lithospheric mantle. Statistically, the buoyancy of the European crust older than 100 Ma varies within a very narrow band of 4.4–4.7 km and is age-independent (Fig. 8c–d). For Cenozoic crust, which is both thin and light (Fig. 4a, e), crustal buoyancy is only 3.65 km. On the whole, the crustal contribution is high in regions with either a very thick crust or with a very light crust (compare with Figs. 2b, 3b, 7b). The former include the Finnish part of the Baltic Shield and some parts of Sarmatia (with parts of the Ukrainian Shield) and Volga-Uralia. The latter include regions with a thick sedimentary cover (the Peri-Caspian basin and the Dnieper–Donets rift), with high lithospheric temperatures, or with a thin (or missing) high-density lower crust (the Phanerozoic Europe and the Pechora basin).

## 7.3. Buoyancy of the subcrustal lithosphere

The isostatic contribution of the lithospheric mantle to the surface topography (Eqs. (2)–(4), Fig. 8a–b) is calculated from data on its thickness and temperature for

two density models: the constant SPT density of 3390 kg/m<sup>3</sup> and the age-dependent SPT density of the lithospheric mantle as constrained by petrologic data on mantle-derived xenoliths from different continents (Fig. 4f) (e.g. Griffin et al., 1998).

### 7.3.1. $B_l$ for constant SPT density of the subcrustal lithosphere

For a constant SPT mantle density, buoyancy of the lithospheric mantle reflects chiefly lithosphere thickening with age, since the density contrast between the lithospheric mantle and the asthenosphere depends only on temperature (which, in turn, controls lithospheric thickness) (Fig. 4d, Eq. (2)). For a constant SPT density of 3390 kg/m<sup>3</sup>, the average *in situ* density of the European lithospheric mantle is 3278±90 kg/m<sup>3</sup>, with regional variations ranging from 3240 to 3300 kg/m<sup>3</sup> (Table 1). In this case, lithospheric buoyancy is always negative and, following the age trend for the lithospheric thickness, decreases with age from *ca.* –1.0 km in Meso-Cenozoic regions to –2.2 km in the Archean shields (Fig. 8c, Table 1). The lowest values (<–3.0 km) are calculated for the Archean blocks where lithosphere thickness exceeds 250 km (Fig. 9c, compare with Fig. 3d). A transition from the cratonic to non-cratonic lithosphere is marked by a sharp change in lithospheric buoyancy: in Meso-Cenozoic regions with a thin lithosphere, lithospheric contribution to the surface topography becomes close to zero (Fig. 9c). Note that even Cenozoic collisional orogens with a large lithospheric thickness associated with subduction zones (e.g. the Alps) have low lithospheric buoyancy due to cold mantle temperatures.

### 7.3.2. $B_l$ for age-dependent density of the subcrustal lithosphere

For the model with a depleted low-density composition of the cratonic lithospheric mantle with an age-dependent density (Fig. 7c), the isostatic contribution of the sublithospheric mantle is very sensitive to variations in lithospheric density (Figs. 8b and 9e, compare with Fig. 7c) and can have both positive and negative sign (Table 1). Despite low lithospheric temperatures, cratonic regions with a depleted low-dense lithosphere have the largest, slightly positive, contribution to the lithospheric buoyancy. However, the isopycnal hypothesis of Jordan (1988, 1997), which assumes that cratonic lithosphere is gravitationally stable due to an approximate balance between compositional and temperature-induced density variations in the lithospheric column, is not entirely satisfied (Fig. 9e), although the amplitude of deflections of lithospheric buoyancy from zero is much smaller than for the model with the constant SPT density (Fig. 9c).

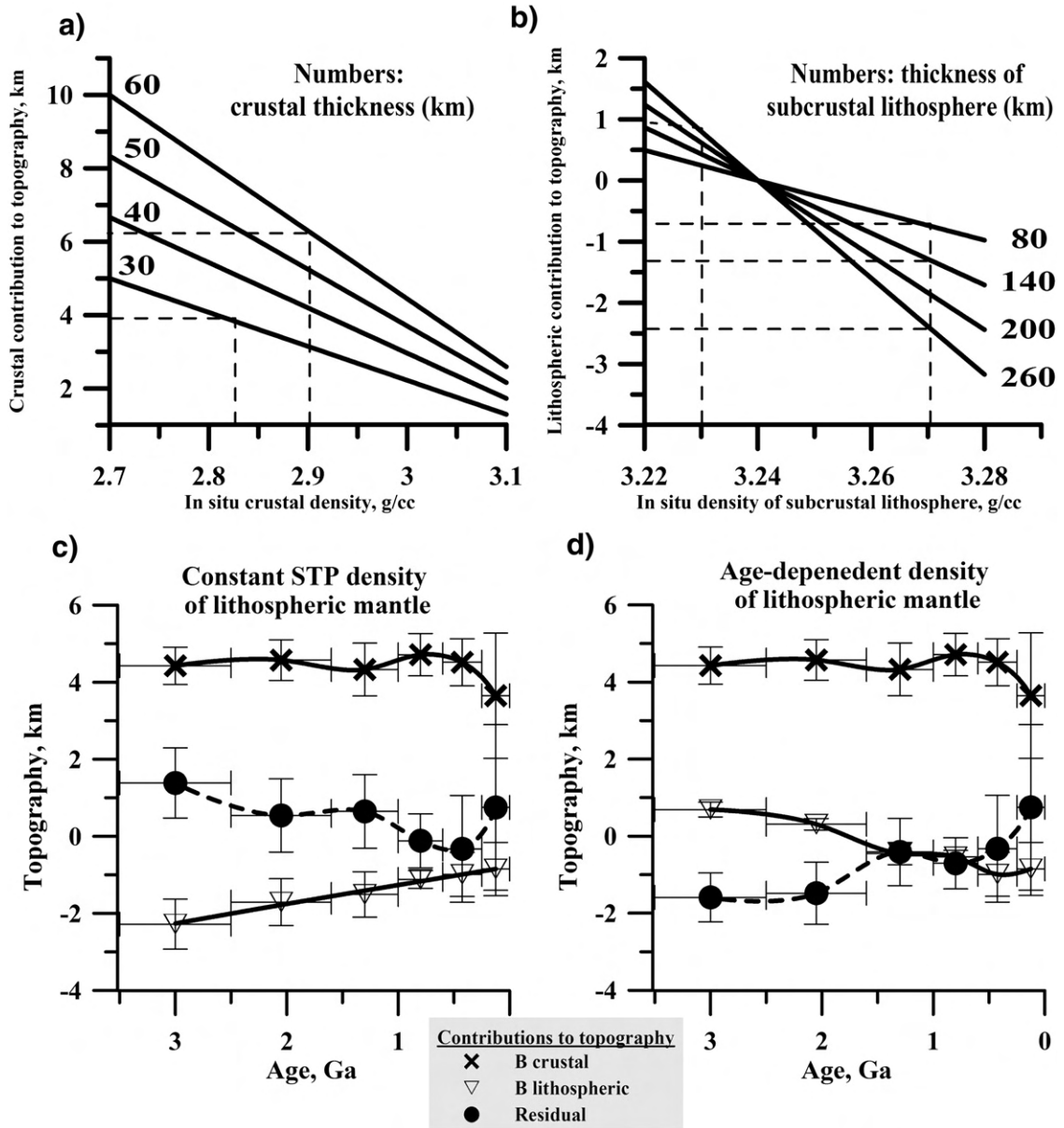


Fig. 8. Crustal and lithospheric contributions to surface topography. (a–b). Effect of *in situ* density variations (a) in the crust and (b) in the lithospheric mantle on crustal and lithospheric buoyancy as a function of crustal and lithospheric thickness (Eqs. (1) and (2)). For typical values of crustal and lithospheric densities (Table 1), crustal buoyancy is in the range from 4 to 6 km, while buoyancy of the lithospheric mantle varies from *ca.* +1 km to –2.5 km (dashed lines). *In situ* density of asthenosphere is 3240 kg/m<sup>3</sup>. (c–d). Crustal, lithospheric and dynamic (residual) contributions to the European topography for the regions of different tectono-thermal age, assuming: (c) constant (3390 kg/m<sup>3</sup>) and (d) age-dependent SPT density of the lithospheric mantle (compare with Fig. 4f). See text for explanations.

Lithospheric buoyancy increases with age from weakly negative values (–0.5–1.3 km) in regions younger than 1.6 Ga to weakly positive values (+0.3+1.0 km) in the Archean-Paleoproterozoic blocks (Figs. 8d and 9e). Note that Proterozoic rifts within the EEC are marked by slightly negative lithospheric buoyancy. For Paleozoic and Meso-Cenozoic structures with fertile lithospheric

mantle the results are the same as for the constant SPT mantle density (Fig. 8c).

#### 7.4. Residual and dynamic topography

Knowledge of the isostatic contributions of the crust and the lithospheric mantle to the observed surface

topography allows calculation of the residual topography, *i.e.* the topography which cannot be explained by thermal and density structure of the lithosphere (Eq. (5)). The residual topography can include two parts: (a) anomalies (artifacts) associated with unaccounted variations in lithospheric properties (chiefly, density of the lithospheric mantle) and (b) the dynamic topography caused by the mantle flow due to density variations in the sublithospheric mantle (Hager et al., 1985). The latter is of a special interest since it provides important information on global and regional mantle dynamics. For example, excess topography in South Africa can be explained by vertical stresses at the lithospheric base caused by an upwelling mantle flow from the lower mantle (Lithgow-Bertelloni and Silver, 1998).

Numerous attempts to estimate the dynamic topography show a huge discrepancy in its value, mainly associated with the poorly known density structure of the lithosphere (*e.g.* Le Stunff and Ricard, 1995). Models of mantle convection and models constrained by seismic tomography predict a dynamic topography of  $>1.5$  km (*e.g.* Hager et al., 1985; Forte et al., 1993), isostatic constraints based on geoid and mantle flow models provide much smaller values (Cazenave et al., 1989; Lithgow-Bertelloni and Silver, 1998), while models based on Cenozoic subsidence and Phanerozoic flooding of continental platforms predict values of *ca.* 0.2 km only (Gurnis, 1990; Lithgow-Bertelloni and Gurnis, 1997). Furthermore, Colin and Fleitout (1990) estimate the amplitude of dynamic topography to be zero.

In the present study the residual (and therefore, the dynamic) topography is calculated directly as the difference between the total surface topography signal and the isostatic contributions of the crust and lithospheric mantle (Eq. (5)). Since two end-member density models were used to calculate lithospheric buoyancy, two end-member models for the residual (dynamic) topography are presented here.

#### 7.4.1. Constant SPT density of the subcrustal lithosphere

Statistically, the crustal contribution to the surface topography is similar for tectonic structures of different ages (Fig. 8c). As a result, for the constant ( $3390 \text{ kg/m}^3$ ) SPT density of the lithospheric mantle, the residual topography (Fig. 9d) largely reflects variations in lithospheric buoyancy, which in turn are controlled chiefly by variations in lithospheric thickness (compare with Figs. 3d and 9c). The residual topography is positive for lithosphere older than 1.0 Ga and younger than 100 Ma, but slightly negative for the Paleozoic and Neoproterozoic structures (Fig. 8c, Table 1).

A significant part of the residual topography can be attributed to compositional variations in the cratonic lithospheric mantle since the largest positive anomalies are observed in the Archean blocks. Positive values of residual topography (*ca.* 1.4 km for the Archean regions and *ca.* 0.6 km for the Meso- and Paleoproterozoic regions, Table 1) can be reduced to zero if the *in situ* density of the lithospheric mantle is  $3260 \text{ kg/m}^3$  (implying a *ca.* 1% density deficit) both in the Archean and in the Meso-Paleoproterozoic blocks. Note that (a) this value of density deficit (depletion) for the Archean cratons is significantly lower than indicated by xenolith data from the Archean cratons of the world (1.3–1.5%, Poudjom Djomani et al., 2001); (b) statistically, the data do not require any difference in density between the Archean and Meso-Paleoproterozoic lithospheric mantle since the difference in lithospheric thickness in these regions effectively compensates for the difference in the residual topography values. For example, the Riphean Central Russian Rift System (Fig. 1b), which has close to zero values of the residual topography, may have the same composition (density) of the Archean-Paleoproterozoic lithospheric mantle as most of Baltica, Sarmatia, and Volga-Uralia, where thicker lithosphere results in higher values of the residual topography.

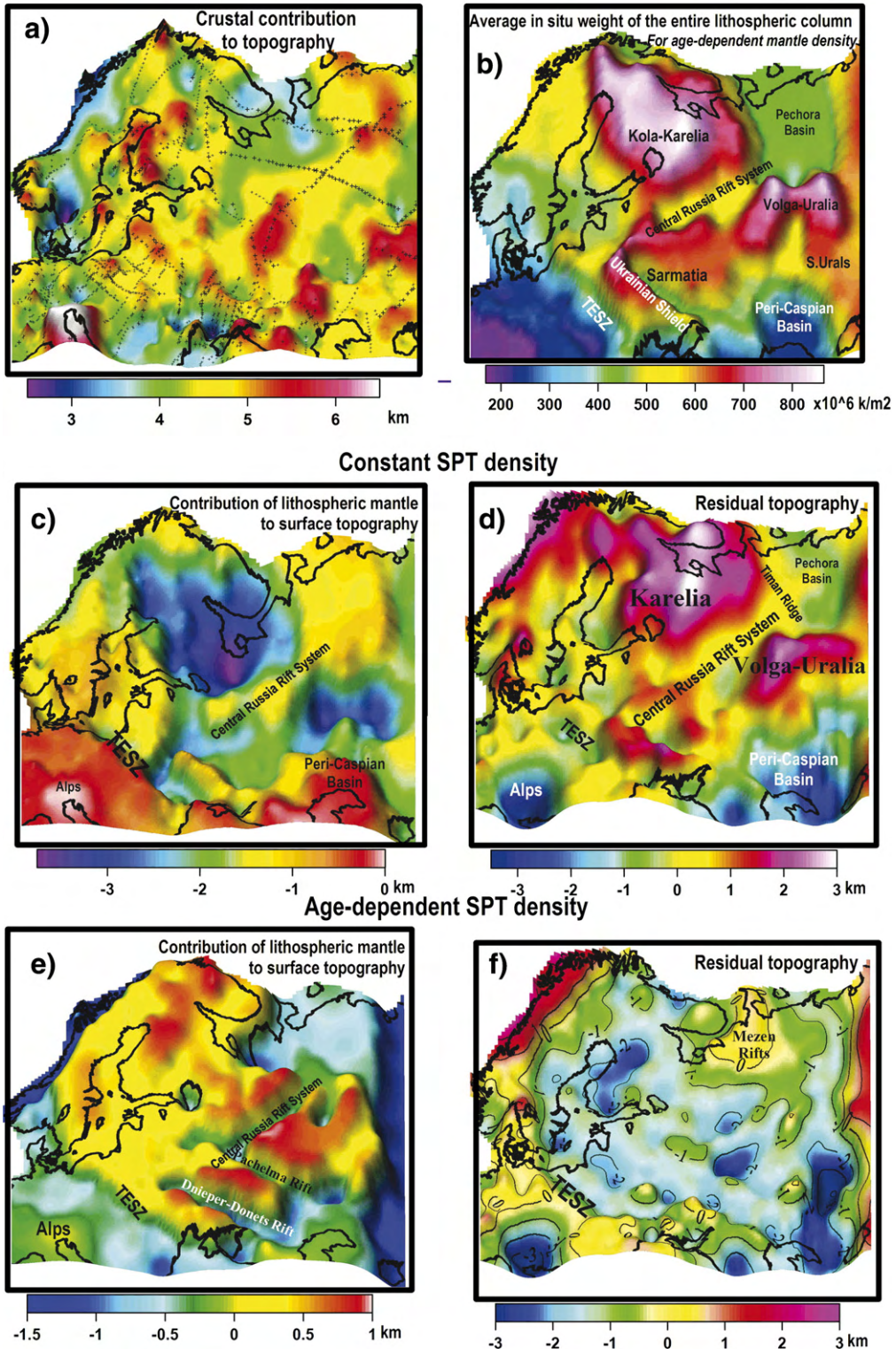
The statistical analysis shows that Meso-Cenozoic regions are characterized by a weakly positive residual topography (0.75 km, Table 1, Fig. 8c), which reflects either the dynamic effect of mantle flow (including large-scale and small-scale convective upwellings and the dynamic support of mantle plumes) in regions of active present-day tectonics, or flexural adjustment of the lithospheric plate in the regions of Phanerozoic tectonics, or density of the lithospheric mantle lower than assumed (*e.g.* due to a presence of partial melts). However, note that many Phanerozoic structures have strong negative anomalies of the residual topography ( $-2$ – $-3$  km as in the Po basin, the Peri-Caspian basin, the southern Peri-Urals foredeep, and in the Northern Caucasus foredeep). These anomalies can reflect the dynamic response (down-flexure) of the lithospheric plates to the down-pull by dense cold subducting slabs (Gurnis, 1992; Stern and Holt, 1994) beneath the Alps and the southern-eastern margins of the EEP.

#### 7.4.2. Age-dependent density of the subcrustal lithosphere

For the age-dependent SPT density of the lithospheric mantle, the contribution of the lithospheric mantle to the surface topography increases with age from weakly negative values in regions younger than 1.6 Ga to

weakly positive values in the Archean-Paleoproterozoic blocks (Fig. 8d). As a result, the residual topography is negative for crustal blocks older than 1.6 Ga

(–1.0–2.0 km) and is close to zero for Meso- and Paleoproterozoic lithosphere (Fig. 9f). Since the results for western Europe are the same as in case of a constant



SPT lithospheric density (Fig. 9d), they are not discussed in this section.

An analysis of the regional patterns shows fascinating results. Two regions of a recent enigmatic tectonic uplift at the cratonic margins, the Norwegian Caledonides (Japsen and Chalmers, 2000) and the Urals (Lider, 1976), show the highest residual topography (>2 km). It can be attributed to a dynamic support of the sublithospheric mantle produced by an upwelling mantle flow. In particular, the density anomaly in the North Atlantic mantle associated with the Iceland plume can provide a dynamic support for the Norwegian Caledonides. The origin of a dynamic support beneath the Uralides is less clear; however, a kinematic analysis of global plate motions for the last 120 Ma predicts a dynamic rebound (uplift) of continents after the cessation of subduction (Lithgow-Bertelloni and Richards, 1998). Further discussion of the origin of a dynamic support of the Norwegian Caledonides and the Urals is outside the scope of the present study. Other regions with a slightly positive residual topography include the Mezen and the Dnieper–Donets Rift systems. In these regions the residual topography is likely to have a dynamic origin, indicating thermo-mechanical (flexural) adjustments of lithospheric plates in regions where active tectonics has ceased in the Paleozoic to Mesozoic.

Another intriguing result of this study is the negative residual topography (*ca.* –1.5 km) of the Archean-Paleoproterozoic blocks of the EEC (Figs. 8d and 9f), although compositional variations in the lithospheric mantle of the EEC have been incorporated into the model. It means that crustal buoyancy together with large lithospheric buoyancy due to high mantle depletion predict the surface topography to be *ca.* 1.5 km higher than is observed within the EEC. A downpull of the lithosphere is required to compensate for this discrepancy. Furthermore, such a downpull should lead to platform subsidence. Indeed, the western and southern parts of the EEC have been subsiding since the Late Paleozoic (Fig. 1, f–h). Note that the region

with the strongest negative residual topography (Bashkiria) has the fastest subsidence rate, as evidenced by Phanerozoic sediments exceeding 5 km in thickness (Fig. 1h).

Two alternative mechanisms can provide the required lithospheric downpull and explain the strong negative residual topography of the Archean-Paleoproterozoic blocks of the EEC: (1) compositionally-induced subsidence due to high lithospheric density or (2) dynamic subsidence (*i.e.* dynamic contribution to the surface topography) due to mantle flow in the sublithospheric mantle. In an earlier study (Artemieva, 2003), it was proposed that the lithospheric mantle of the southern EEC has a non-cratonic, high-density that causes compositionally-induced low topography of this region. The results of the present study, in which residual (dynamic) and lithospheric contributions to the surface topography are separated, provide further insight into this problem.

(1) Compositional subsidence means that the assumed density deficit in the cratonic mantle (constrained by petrologic studies of mantle peridotites) is overestimated. Zero residual topography of the Archean-Paleoproterozoic blocks of the EEC can be achieved if the degree of depletion of their lithospheric mantle is significantly lower (*ca.* 0.9–1.0%) than estimated for other Archean cratons from xenolith data (Griffin *et al.*, 1998; Poudjom Djomani *et al.*, 2001). For example, Fe-rich dunites and wehrlites can be undersampled by xenoliths due to their high densities (0.6%–3% higher than densities of peridotites) (Lee and Rudnick, 1997), resulting in too low values of the density of the cratonic lithosphere as constrained by peridotites from mantle-derived xenoliths. An alternative explanation, which requires that lithospheric geotherms in the EEC are systematically much colder than assumed in the present study, is supported neither by surface heat flow data nor by xenolith P–T arrays from Arkhangelsk and Karelia (Kukkonen and Peltonen, 1999; Malkovets *et al.*, 2003).

Recent petrologic studies support the hypothesis of a negative compositional buoyancy of some Archean-

Fig. 9. Crustal, lithospheric, and dynamic contributions to the surface topography of the EEC. Data sources same as for Figs. 2 and 3. (a) Crustal contribution to surface topography. Dots show locations of some of the seismic profiles used in the present study. (b) Average *in situ* weight of the entire lithospheric column (calculated from average *in situ* density and thickness of the crust and lithospheric mantle and assuming compositional density variations in the latter, Figs. 2b, 3d, 7b,c). The map provides basis for interpretations of gravity anomalies. (c) Lithospheric contribution to the surface topography for a constant (3390 kg/m<sup>3</sup>) SPT density of the lithospheric mantle. The map effectively reflects variations in the lithospheric thickness (compare with Fig. 3d). (d) Residual (dynamic) topography for a constant (3390 kg/m<sup>3</sup>) SPT density of the lithospheric mantle (a difference between surface topography (corrected for the constant  $\Delta$ , Eq. (5)) and Fig. 9a and c). Since, statistically, crustal contribution to the surface topography is similar for tectonic structures of different ages (Fig. 8c), the map largely reflects variations in the lithospheric thickness and buoyancy (compare with Figs. 3d and 9c). (e) Lithospheric contribution to the surface topography for the age-dependent SPT density of the lithospheric mantle. The map reflects variations in the lithospheric density (Fig. 7c). Despite low temperatures, cratonic regions with depleted low-density lithosphere have the largest contribution to lithospheric buoyancy. (f) Residual (dynamic) topography for the age-dependent SPT density of the lithospheric mantle (the difference between the surface topography (corrected for the constant  $\Delta$ , Eq. (5)) and Fig. 9a and e). Note high standing of the Norwegian and the Urals mountains and negative values for most of the EEC.

Paleoproterozoic regions of the world. Indeed, they indicate that typically the subcrustal lithosphere of the cratons is vertically stratified: lithospheric depletion decreases with depth and is the lowest in its basal parts (Gaul et al., 2000). This leads to an increase of the lithospheric density with depth. According to the isopycnic hypothesis (Jordan, 1988, 1997), an approximate balance between compositional and temperature-induced density variations in the lithospheric column should make the entire cratonic lithosphere gravitationally stable. However, recent experimental studies of Kaapvaal garnet lherzolites and Tanzanian peridotite xenoliths (Boyd et al., 1999; Lee and Rudnick, 1999) indicate that many peridotites from depths greater than 120 km are much denser than predicted by the isopycnic hypothesis. Conversely, the estimates of Poudjom Djomani et al. (2001) for typical cratonic geotherms and lithospheric densities calculated from modal compositions suggest that only the lower (below 100–150 km depth) part of the cratonic lithosphere is buoyant with respect to the underlying mantle. Despite the principal discrepancy between these two sets of results, both of them imply that cratonic lithosphere can be negatively buoyant due to its vertical compositional heterogeneity and density stratification. In particular, in those parts of the EEC, that were affected by Phanerozoic tectono-magmatic activity, fertile components brought by ascending basaltic magmas may have increased the density of the lower lithosphere (Lee and Rudnick, 1997), causing its negative residual (in this case, compositional) buoyancy (Artemieva, 2003).

(2) If petrologic data provides accurate constraints on the density structure of the lithospheric mantle, the strong negative residual topography in the Archean-Paleoproterozoic blocks of the EEC (Figs. 8d and 9f) must be attributed to dynamic subsidence (dynamic topography), e.g. to a convective downflow in the sublithospheric mantle. Spatial variations in the amplitude of the dynamic topography apparently do not correlate with tectonic units of the EEC, but seem to be a craton-scale feature, complicated by regional patterns. Indeed, significant lateral variations in the depth to the lithosphere–asthenosphere boundary beneath the EEC presumably affect the pattern of mantle convection near the lithospheric base and may cause small-scale convectional instabilities around regions with large gradients in lithospheric thickness. Large-scale mantle downwellings beneath the Archean-Paleoproterozoic blocks of the EEC will effectively divert heat from the mantle, leading to long-term stability and survival of the ancient continental lithosphere. The lack of high-resolution tomography models for the mantle of the

EEC precludes further speculation on the origin of its dynamic topography.

## 8. Conclusions

The analysis of a large volume of regional seismic reflection/refraction data, seismic tomography interpretations, and thermal data indicate that the EEC is characterized by huge undulations in the relief of the top of the basement (20+ km), the Moho (ca. 30 km), and the lithosphere–asthenosphere boundary (200+ km). This paper examines the isostatic contributions of the crust, the subcrustal lithosphere, and the sublithospheric mantle (dynamic topography) to the surface topography, which does not exceed 200 m for most of the EEC.

1. The statistical analysis of the crustal structure of the EEC indicates a systematic increase in average crustal density with age, from the Phanerozoic to the Archean, coupled with a systematic increase in the depth to Moho and thickness of the crystalline crust; however it is the Paleoproterozoic crust that has the largest crustal densities and thickness. *In situ* density contrast between the crystalline crust and the sublithospheric upper mantle varies from ca. 500 kg/m<sup>3</sup> for Phanerozoic blocks to 150–250 kg/m<sup>3</sup> for Archean-Paleoproterozoic shields.
2. A highly heterogeneous thermal regime of the cratonic upper mantle is expressed in significant variations in the lithospheric thermal thickness, that increases almost linearly with age and reaches the largest values in the Archean terranes. An analysis of large-scale P- and S-wave seismic tomography models (Bijwaard and Spakman, 2000; Shapiro and Ritzwoller, 2002; Piromallo and Morelli, 2003) at 100, 150, 200, and 250 km depths does not show any age-dependence of Vp/Vs ratio for the Precambrian lithosphere, suggesting that while Vp/Vs ratio can be effectively used to outline the cratonic margins, it is not sensitive to velocity and compositional variations within the cratonic lithosphere.
3. Buoyancy analysis indicates that isostatic contribution of the crust to the surface topography does not depend on the age for the crust older than 100 Ma and is ca. 4.5 km. On the contrary, lithospheric buoyancy shows a strong age-dependence. For the constant SPT (i.e. at room conditions) density of the lithospheric mantle, its buoyancy reflects chiefly lithosphere thickening with age. For the age-dependent SPT density of the lithospheric mantle, as constrained by petrologic data on mantle-derived

xenoliths from different continents, its buoyancy is controlled chiefly by its density structure: cratonic regions with a depleted low-density lithospheric mantle have the largest (slightly positive) contribution to the lithospheric buoyancy despite their low lithospheric temperatures. Due to cold mantle temperatures, Cenozoic collisional orogens associated with subduction zones have low lithospheric buoyancy despite their large lithospheric thickness.

4. Residual topography calculated for a constant SPT density of the lithospheric mantle requires that the density deficit in the Precambrian lithospheric mantle of different ages is the same, *ca.* 1%. For the Archean cratons, this value is significantly lower than constrained by petrologic studies of mantle-derived peridotites. For the age-dependent SPT density of the lithospheric mantle, negative residual topography suggests either compositional subsidence of the EEC due to its high lithospheric density or the dynamic subsidence in response to mantle downflow caused by density anomalies in the sublithospheric mantle. In the former case, the isopycnic hypothesis is not entirely satisfied for the cratonic lithosphere of Europe. In the latter case, mantle downflow beneath the Archean-Paleoproterozoic cratons (as exemplified by the EEC) will effectively divert heat from the lithospheric roots, providing unique conditions for their long-term survival.

In Phanerozoic regions, the results are independent of the assumptions on the lithospheric density. Negative (–2–3 km) dynamic topography in the Po basin, the Peri-Caspian basin, the Northern Caucasus foredeep (and, perhaps, in the southern part of the Peri-Urals foredeep) is likely to reflect down-flexure of the lithospheric plates in response to down-pull by subducting slabs. The strongest positive residual topography (>2 km) calculated for the Norwegian Caledonides and the Urals can be attributed to a dynamic support of the sublithospheric mantle.

## Acknowledgements

The paper summarizes the results presented at the TopoEurope workshop, Heidelberg, October 2005. The study benefited from the discussions with D. Bercovici and S.V. Sobolev, which provided further insights into the problem. Thorough reviews of E.B. Burov and, in particular, of P.A. Ziegler are gratefully acknowledged. Comments of H. Thybo on an early version of the manuscript are appreciated. The study is supported by a personal research grant from Carlsbergfondet, Denmark.

## References

- Alinaghi, A., Bock, G., Kind, R., Hanka, W., Wylegalla, K., TOR and SVEKALAPKO groups, 2003. Receiver function analysis of the crust and upper mantle from the North German Basin to the Archean Baltic Shield. *Geophys. J. Int.* 155, 641–652.
- Anderson, D.L., 1987. Thermally induced phase changes, lateral heterogeneity of the mantle, continental roots, and deep slab anomalies. *J. Geophys. Res.* 92, 13968–13980.
- Anderson, D.L., 1989. *Theory of the Earth*. Blackwell Scientific Publication, Boston. 366 pp.
- Artemieva, I.M., 2003. Lithospheric structure, composition, and thermal regime of the East European craton: implications for the subsidence of the Russian Platform. *Earth Planet. Sci. Lett.* 213, 429–444.
- Artemieva, I.M., 2006. Global  $1^\circ \times 1^\circ$  thermal model TC1 for the continental lithosphere: implications for lithosphere secular evolution. *Tectonophysics* 416, 245–277.
- Artemieva, I.M., Mooney, W.D., 2001. Thermal structure and evolution of Precambrian lithosphere: a global study. *J. Geophys. Res.* 106, 16387–16414.
- Artemieva, I.M., Thybo, H., Kaban, M.K., 2006. Deep Europe today: geophysical synthesis of the upper mantle structure and lithospheric processes over 3.5 Ga. *Geol. Soc. London Sp. Publ.*, vol. 32, pp. 11–41.
- BABEL Working Group, 1993. Deep seismic reflection/refraction interpretation of crustal structure along BABEL profiles A and B in the southern Baltic Sea. *Geophys. J. Int.* 112, 325–343.
- Bayer, U., Grad, M., Pharaoh, T.C., Thybo, H., Guterch, A., Banka, D., Lamarche, J., Lassen, A., Lewerenz, B., Scheck, M., Marotta, A.-M., 2002. The southern margin of the East European Craton: new results from seismic sounding and potential field between the North Sea and Poland. *Tectonophysics* 360, 301–314.
- Bijwaard, H., Spakman, W., 2000. Non-linear global P-wave tomography by iterated linearized inversion. *Geophys. J. Int.* 141, 71–82.
- Bock, G., The SVEKALAPKO Seismic Tomography Working Group (SSTWG), 2001. Seismic probing of the Fennoscandian lithosphere. *EOS Trans. AGU* 82 (621), 628–629.
- Boyd, F.R., 1989. Compositional distinction between oceanic and cratonic lithosphere. *Earth Planet. Sci. Lett.* 96, 15–26.
- Boyd, F.R., Pearson, D.G., Nixon, P.H., Mertzman, S.A., 1993. Low-calcium garnet harzburgites from Southern Africa; their relations to craton structure and diamond crystallization. *Contrib. Mineral. Petrol.* 113 (3), 352–366.
- Boyd, F.R., Pearson, D.G., Mertzman, S.A., 1999. Spinel-facies peridotites from the Kaapvaal root. In: Gurney, J.J., Gurney, J.L., Pascoe, M.D., Richardson, S.H. (Eds.), *Proc. 7th Intern. Kimberlite Conf.*, vol. 1, pp. 40–48.
- Bronguleev V.V.(Ed.), 1986. Map of the pre-Riphean basement upper surface depth of the East-European platform. Scale 1:5 000 000. USSR Ministry of Geology, Moscow.
- Bruneton, M., Pedersen, H.A., Vacher, P., Kukkonen, I.T., Arndt, N.T., Funke, S., Friederich, W., Farra, V., 2004a. The SVEKALAPKO Seismic Tomography Working Group, layered lithospheric mantle in the central Baltic Shield from surface waves and xenolith analysis. *Earth Planet. Sci. Lett.* 226, 41–52.
- Bruneton, M., Pedersen, H.A., Farra, V., Arndt, N.T., Vacher, P., 2004b. The SVEKALAPKO Seismic Tomography Working Group, complex lithospheric structure under the central Baltic Shield from surface wave tomography. *J. Geophys. Res.* 109, B10303.
- Burov, E.B., Diament, M., 1995. The effective elastic thickness ( $T_e$ ) of continental lithosphere: what does it really mean? *J. Geophys. Res.* 100, 3905–3927.

- Carbonell, R., Gallart, J., Perez-Estaun, A., Diaz, J., Kashubin, S., Mechie, J., Wenzel, F., Knapp, J., 2000. Seismic wide-angle constraints on the crust of the southern Urals. *J. Geophys. Res.* 105 (B6), 13755–13777.
- Cazenave, A., Souriau, A., Dominh, K., 1989. Global coupling of earth surface topography with hotspots, geoid and mantle heterogeneities. *Nature* 340, 54–57.
- Christensen, N., Mooney, W., 1995. Seismic velocity structure and composition of the continental crust: a global view. *J. Geophys. Res.* 100, 9761–9788.
- Cloetingh, S., Ziegler, P.A., Beekman, F., Andriessen, P.A.M., Matenco, L., Bada, G., et al., 2005. Lithospheric memory, state of stress and rheology: neotectonic controls on Europe's intraplate continental topography. *Quat. Sci. Rev.* 24, 241–304.
- Clowes, R.M., Cook, F.A., Ludden, J.N., 1998. LITHOPROBE leads to new perspectives on continental evolution. *GSA Today* 8, 1–7.
- Colin, P., Fleitout, L., 1990. Topography of the ocean floor: thermal evolution of the lithosphere and interaction of the deep mantle heterogeneity with the lithosphere. *Geophys. Res. Lett.* 17, 1961–1964.
- Cook, F.A., van der Velden, A.J., Hall, K.W., Roberts, B.J., 1999. Frozen subduction in Canada's Northwest Territories: lithoprobe deep lithospheric reflection profiling of the western Canadian Shield. *Tectonics* 18, 1–26.
- DOBREFraction'99 Working Group, 2003. "DOBREFraction'99"-velocity model of the crust and upper mantle beneath the Donbas Foldbelt (East Ukraine). *Tectonophysics* 371, 81–110.
- Durrheim, R.J., Mooney, W.D., 1991. Archean and Proterozoic crustal evolution — evidence from crustal seismology. *Geology* 19 (6), 606–609.
- Egorin, A.V., 1998. Velocity structure, composition and discrimination of crustal provinces in the former Soviet Union. *Tectonophysics* 298 (4), 395–404.
- EUROBRIDGE Seismic Working Group, 1999. Seismic velocity structure across the Fennoscandia–Sarmatia suture of the East European Craton beneath the EUROBRIDGE profile through Lithuania and Belarus. *Tectonophysics* 314, 193–217.
- EUROBRIDGE Seismic Working Group, 2000. EUROBRIDGE'97: modelling of S-waves field on the EB'97 seismic profile. *Geophys. J. (Kiev)* 22, 87–88.
- EUROBRIDGE Working Group and EUROBRIDGE'95, 2001. Deep seismic profiling within the East European Craton. *Tectonophysics* 339, 153–175.
- Forte, A., Peltier, W., Dziewonski, A., Woodward, R., 1993. Dynamic surface topography: a new interpretation based upon mantle flow models derived from seismic tomography. *Geophys. Res. Lett.* 20, 225–228.
- Gaul, O.F., Griffin, W.L., O'Reilly, S.Y., Pearson, N.J., 2000. Mapping olivine composition in the lithospheric mantle. *Earth Planet. Sci. Lett.* 182, 223–235.
- Gorbatshev, R., Bogdanova, S., 1993. Frontiers in the Baltic Shield. *Precambrian Res.* 64, 3–21.
- Grad, M., Tripolsky, A., 1995. Crustal structure from P and S seismic waves and petrologic model of the Ukrainian shield. *Tectonophysics* 250, 89–112.
- Grad, M., Keller, G.R., Thybo, H., Guterch, A., POLONAISE Working Group, 2002. Lower lithospheric structure beneath the Trans-European Suture Zone from POLONAISE'97 seismic profiles. *Tectonophysics* 360, 153–168.
- Grad, M., Guterch, A., Keller, G.R., et al., 2006. Lithospheric structure beneath trans-Carpathian transect from Precambrian platform to Pannonian basin: CELEBRATION 2000 seismic profile CEL05. *J. Geophys. Res.* 111 (B3), B03301.
- Griffin, W.L., O'Reilly, S.Y., Ryan, C.G., Gaul, O., Ionov, D., 1998. Secular variation in the composition of subcontinental lithospheric mantle. In: Braun, J., et al. (Eds.), *Structure and evolution of the Australian continent*. AGU Geodynam. Ser., vol. 26, pp. 1–25.
- Griffin, W.L., O'Reilly, S.Y., Ryan, C.G., 1999. The composition and origin of subcontinental lithospheric mantle. In: Fei, Y., Bertka, C.M., Mysen, B.O. (Eds.), *Mantle petrology: field observations and high pressure experimentation: a tribute to Francis R. (Joe) Boyd*. *Geochem. Soc. Spec. Publ.*, vol. 6, pp. 13–45.
- Gurnis, M., 1990. Bounds on global dynamic topography from Phanerozoic flooding of continental platforms. *Nature* 344, 754–756.
- Gurnis, M., 1992. Rapid continental subsidence following the initiation and evolution of subduction. *Science* 255, 1556–1558.
- Hafkenscheid, E., Wortel, M.J.R., Spakman, W., 2006. Subduction history of the Tethyan region derived from seismic tomography and tectonic reconstructions. *J. Geophys. Res.* 111, B08401. doi:10.1029/2005JB003791.
- Hager, B., Clayton, R., Richards, M., Comer, R., Dziewonski, A., 1985. Lower mantle heterogeneity, dynamic topography and the geoid. *Nature* 313, 541–545.
- Hamilton, W., 1970. The Uralides and the motion of the Russian and Siberian platforms. *Geol. Soc. Amer. Bull.* 81, 2553–2576.
- Ilichenko, T.V., Bukharev, V.P., 2001. Velocity model of the crust and the uppermost mantle of the Korosten Pluton (Ukrainian Shield) and its geological interpretation (along DSS Shepetovka–Chernigov profile). *Geophys. J. (Kiev)* 23, 72–82.
- Irfune, T., 1987. An experimental investigation of the pyroxene–gamet transformation in a pyrolyte composition and its bearing on the composition of the mantle. *Phys. Earth Planet. Inter.* 45, 324–336.
- Janik, T., Grad, N., Guterch, A., et al., 2005. Lithospheric structure of the Trans-European Suture Zone along the TTZ–CEL03 seismic transect (from NW to SE Poland). *Tectonophysics* 411 (1–4), 129–156.
- Japsen, P., Chalmers, J.A., 2000. Neogene uplift and tectonics around the North Atlantic: overview. *Glob. Planet. Change* 24, 165–173.
- Jordan, T.H., 1979. Mineralogies, densities and seismic velocities of gamet lherzolites and their geophysical implications. In: Boyd, F.R., Meyer, H.O.A. (Eds.), *The mantle sample: inclusions in kimberlites and other volcanics*. *Proc. 2nd Intern. Kimberlite Conf.*, vol. 2, pp. 1–14.
- Jordan, T.H., 1981. Continents as a chemical boundary layer. *Philos. Trans. R. Soc. Lond. Ser. A: Math. Phys. Sci.* 301, 359–373.
- Jordan, T.H., 1988. Structure and formation of the continental tectosphere. *J. Petrol.* 29, 11–37.
- Jordan, T.H., 1997. Petrologic controls on the density and seismic velocities of the cratonic upper mantle. *EOS Trans. AGU* 78 (46), F746.
- Kaban, M., 2001. A gravity model of the North Eurasia crust and upper mantle: 1. Mantle and isostatic residual gravity anomalies. *Russ. J. Earth Sci.* 3 (2), 143–163 (<http://www.agu.org/wps/rjes/>).
- Kaban, M.K., 2002. A gravity model of the north Eurasia crust and upper mantle: 2. The Alpine–Mediterranean fold belt and adjacent structures of the southern former USSR. *Russ. J. Earth Sci.* 4 (1), 19–33 (<http://www.agu.org/wps/rjes/>).
- Kaban, M.K., Schwintzer, P., Artemieva, I.M., Mooney, W.D., 2003. Density of the continental roots: compositional and thermal effects. *Earth Planet. Sci. Lett.* 209, 53–69.
- Kennett, B.L.N., Engdahl, E.R., 1991. Traveltimes for global earthquake location and estimation. *Geophys. J. Int.* 105, 429–465.
- Korja, A., Heikkinen, P., 2005. The accretionary Svecofennian orogen — insight from the BABEL profiles. *Precambrian Res.* 136 (3–4), 241–268.
- Korja, A., Heikkinen, P., Aaro, S., 2001. Crustal structure of the northern Baltic Sea paleorift. *Tectonophysics* 331, 341–358.

- Korja, A., Lahtinen, R., Heikkinen, P., Kukkonen, I.T., FIRE Working Group, 2006. Tectonic stacking and collapse of the Svecofennian crust along FIRE profiles. EGU abstracts, Vienna, April 2006, EGU06-A-06767.
- Korsman, K., Korja, T., Pajunen, M., et al., 1999. The GGT/SVEKA transect: structure and evolution of the continental crust in the Paleoproterozoic Svecofennian orogen in Finland. *Int. Geol. Rev.* 41 (4), 287–333.
- Kostyuchenko, S.L., Egorin, A.V., Solodilov, L.N., 1999. Structure and genetic mechanisms of the Precambrian rifts of the East-European Platform in Russia by integrated study of seismic, gravity, and magnetic data. *Tectonophysics* 313, 9–28.
- Kostyuchenko, S.L., Morozov, A.F., Stephenson, R.A., 2004. The evolution of the southern margin of the East European Craton based on seismic and potential field data. *Tectonophysics* 381, 101–118.
- Kozlovskaya, E., Taran, L.N., Yliniemi, J., Giese, R., Karatayev, G.I., 2002. Deep structure of the crust along the Fennoscandia–Sarmatia Junction Zone (Central Belarus): results of a geophysical–geological integration. *Tectonophysics* 358, 97–120.
- Kukkonen, I.T., Peltonen, P., 1999. Xenolith-controlled geotherm for the central Fennoscandian Shield: implications for lithosphere–asthenosphere relations. *Tectonophysics* 304, 301–315.
- Lachenbruch, A.H., Morgan, P., 1990. Continental extension, magmatism and elevation; formal relations and rules of thumb. *Tectonophysics* 174, 39–62.
- Lee, C.T.A., 2003. Compositional variation of density and seismic velocities in natural peridotites at STP conditions: implications for seismic imaging of compositional heterogeneities in the upper mantle. *J. Geophys. Res.* 108 (B9) (art. no. 2441).
- Lee, C.-T., Rudnick, R., 1997. The formation and destruction of cratonic lithosphere: insights from the Tanzanian craton. *EOS Trans. Am. AGU* 78 (46), 746.
- Lee, C.T., Rudnick, R.L., 1999. In: Gurney, J.J., Gurney, J.L., Pascoe, M.D., Richardson, S.H. (Eds.), *Compositionally stratified cratonic lithosphere: petrology and geochemistry of peridotite xenoliths. Proc. 7th Intern. Kimberlite Conf.*, vol. 2, pp. 503–521.
- Le Stunff, Y., Ricard, Y., 1995. Topography and geoid due to lithospheric mass anomalies. *Geophys. J. Int.* 122 (3), 982–990.
- Lider, V.A., 1976. Quaternary Deposits of the Urals, Moscow, Nedra. 144 pp.
- Lithgow-Bertelloni, C., Gurnis, M., 1997. Cenozoic subsidence and uplift of continents from time-varying dynamic topography. *Geology* 25, 735–738.
- Lithgow-Bertelloni, C., Richards, M.A., 1998. The dynamics of Cenozoic and Mesozoic plate motions. *Rev. Geophys.* 36, 27–78.
- Lithgow-Bertelloni, C., Silver, P., 1998. Dynamic topography, plate driving forces and the African superswell. *Nature* 395, 269–272.
- Malkovets, V.G., Taylor, L.A., Griffin, W., O'Reilly, S., Pearson, N., Pokhilenko, N.P., Verichev, E.M., Golovin, N.N., Litasov, K.D., 2003. Cratonic conditions beneath Arkhangelsk, Russia: garnet peridotites from the Grib kimberlite. *Proc. 8th Intern. Kimberlite Conf.*, Victoria, BC, Canada, June 2003, FLA-0220.
- Mitrovica, J.X., Pysklywec, R.N., Beaumont, C., Rutt, A., 1996. The Devonian to Permian sedimentation of the Russian platform; an example of subduction-controlled long-wavelength tilting of continents. *J. Geodyn.* 22, 79–96.
- Morozov, A.F. (Ed.), 2001. Deep structure and geodynamics of the southern Urals (the URALSEIS project). Ministry of Natural Resources of Russia, Tver. 286 pp.
- Nalivkin, V.D., 1976. Dynamics of the development of the Russian platform structures. *Tectonophysics* 36, 247–262.
- Neprochnov, Yu.P., Semenov, G.A., Sharov, N.V., Yliniemi, J., Komminaho, K., Luosto, U., Heikkinen, P., 2000. Comparison of the crustal structures of the Barents Sea and the Baltic Shield from seismic data. *Tectonophysics* 321, 429–447.
- Nevolin, N.V., Kovylin (Eds.), 1993. Geological and geophysical modelling of oil and gas provinces. Moscow, Nedra. 204 pp.
- Nisbet, E.G., 1984. The continental and oceanic crust and lithosphere in the Archean: isostatic, thermal and tectonic models. *Can. J. Earth Sci.* 21, 1426–1441.
- NOAA National Geophysical Data Center, 2001. 2-Minute Gridded Global Relief Data (ETOPO2). NGDC, Boulder, Colorado. [www.ngdc.noaa.gov/mgg/fliers/01mgg04.html](http://www.ngdc.noaa.gov/mgg/fliers/01mgg04.html).
- Nolet, G., Zielhuis, A., 1994. Low S velocities under the Tornquist–Teisseyre zone: evidence from water injection into the transition zone by subduction. *J. Geophys. Res.* 99, 15813–15820.
- Pavlenkova, N.I., 1988. Crustal structure of deep sedimentary continental basins based on seismic data. *Phys. Solid Earth* 24 (4).
- Pavlenkova, N.I., 1996. Crust and upper mantle structure in Northern Eurasia from seismic data. *Adv. Geophys.* 37, 1–133.
- Pearson, D.G., 1999. The age of continental roots. *Lithos* 48, 171–194.
- Pearson, D.G., Carlson, R.W., Shirey, S.B., Boyd, F.R., Nixon, P.H., 1995. Stabilization of Archaean lithospheric mantle; a Re–Os isotope study of peridotite xenoliths from the Kaapvaal Craton. *Earth Planet. Sci. Lett.* 134, 341–357.
- Pérez-Gussinyé, M., Watts, A.B., 2005. The long-term strength of Europe and its implications for plate-forming processes. *Nature* 436, 381–384.
- Piomallo, C., Morelli, A., 2003. P-wave tomography of the mantle under the Alpine–Mediterranean area. *J. Geophys. Res.* 108 (B2) (art. no. 2065).
- Podoba, N.V., Ozerskaya, M.A. (Eds.), 1975. Physical properties of the sedimentary cover of the East-European Platform. Nauka, Moscow.
- Pollack, H.N., Hurter, S.J., Johnson, J.R., 1993. Heat flow from the Earth's interior: analysis of the global data set. *Rev. Geophys.* 31, 267–280.
- Poudjom Djomani, Y.H., O'Reilly, S.Y., Griffin, W.L., Morgan, P., 2001. The density structure of subcontinental lithosphere through time. *Earth Planet. Sci. Lett.* 184, 605–621.
- Poupinet, G., Thouvenot, F., Zolotov, E.E., Matte, P., Egorin, A.V., Rackitov, V.A., 1997. Teleseismic tomography across the middle Urals: lithospheric trace of an ancient continental collision. *Tectonophysics* 276, 19–33.
- Rudnick, R., Fountain, D.M., 1995. Nature and composition of the continental crust: a lower crustal perspective. *Rev. Geophys.* 33, 267–309.
- Sandoval, S., Kissling, E., Ansorge, J., the SVEKALAPKO STWG, 2004. High-resolution body wave tomography beneath the SVEKALAPKO array: II. anomalous upper mantle structure beneath central Baltic Shield. *Geophys. J. Int.* 157, 200–214.
- Shapiro, N.M., Ritzwoller, M.H., 2002. Monte-Carlo inversion for a global shear velocity model of the crust and upper mantle. *Geophys. J. Int.* 151, 1–18.
- Sollogub, V.B., Chekunov, A.V., Garetsky, R.G., et al., 1989. Lithosphere of the Central and Eastern Europe. The East-European Platform. Kiev, Naukova Dumka. 186 pp.
- Sroda, P., Czuba, W., Guterch, A., et al., 1999. P- and S-wave velocity model of the southwestern margin of the Precambrian East European Craton; POLONAISE '97, Profile P3. *Tectonophysics* 314, 175–192.
- Stephenson, R.A. (Ed.), 2004. EUROPROBE, GeoRift 3: Intraplate Tectonics and Basin Dynamics. The Lithosphere of the Southern Eastern European Craton and its Margin. *Tectonophysics*, vol. 381. 273 pp.

- Stern, T.A., Holt, W.E., 1994. Platform subsidence behind an active subduction zone. *Nature* 368, 233–236.
- Thybo, H., Pharaoh, T., Guterch, A. (Eds.), 2002. The Trans European Suture Zone II. *Tectonophysics*, vol. 360. 314 pp.
- Thybo, H., Janik, T., Omelchenko, V.D., et al., 2003. Upper lithospheric seismic velocity structure across the Pripyat Trough and the Ukrainian Shield along the EUROBRIDGE'97 profile. *Tectonophysics* 371, 41–80.
- Tiira, T., Hyvonen, T., Komminaho, K., Korja, A., Heikkinen, P., 2006. 3-D inversion of Moho discontinuity using wide-angle reflections in the Baltic Shield. EGU abstracts, Vienna, April 2006, EGU06-A-06893.
- Wilde-Piorko, M., Grad, M., TOR Working Group, 2002. Crustal structure variation from the Precambrian to Paleozoic Platforms in Europe imaged by the inversion of teleseismic receiver functions — Project TOR. *Geophys. J. Int.* 150, 261–270.
- Wilson, M., Lyashkevitch, Z., 1996. Magmatic evolution and the geodynamics of rifting in the Pripyat–Dnieper–Donets rift. *Tectonophysics* 268, 65–82.
- Yegorova, T.P., Stephenson, R.A., Kozlenko, V.G., Starostenko, V.I., Legostaeva, O.V., 1999. 3-D gravity analysis of the Dniepr–Donets Basin and Donbas Foldbelt, Ukraine. *Tectonophysics* 313, 41–58.
- Yliniemi, J., Tiira, T., Luosto, U., et al., 2001. EUROBRIDGE'95: deep seismic profiling within the East European Craton. *Tectonophysics* 339 (1–2), 153–175.
- Zielhuis, A., Nolet, G., 1994. Deep seismic expression of an ancient plate boundary in Europe. *Science* 265 (5168), 79–81.